

**ACTIVE TUNING OF THERMAL CONDUCTIVITY IN
SINGLE LAYER GRAPHENE PHONONIC CRYSTALS USING
ENGINEERED PORE GEOMETRY AND STRAIN**

by

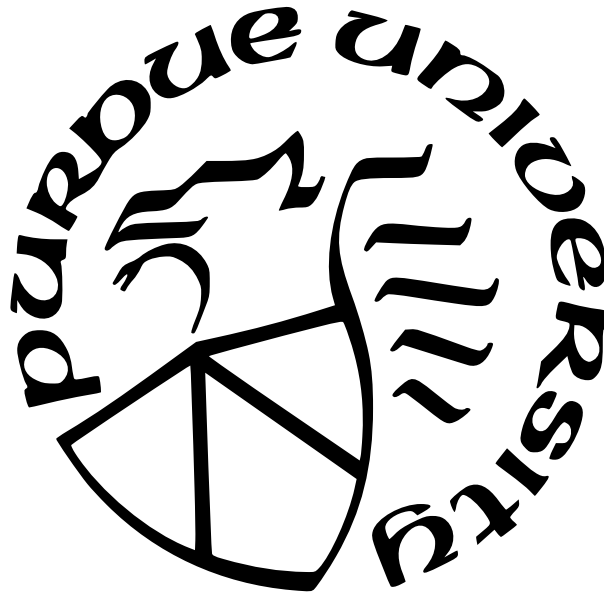
Radhakrishna Korlam

A Thesis

Submitted to the Faculty of Purdue University

In Partial Fulfillment of the Requirements for the degree of

Master of Science in Mechanical Engineering



School of Mechanical Engineering

West Lafayette, Indiana

December 2021

**THE PURDUE UNIVERSITY GRADUATE SCHOOL
STATEMENT OF COMMITTEE APPROVAL**

Dr. Amy Marconnet, Co-Chair

School of Mechanical Engineering

Dr. Fabio Semperlotti, Co-Chair

School of Mechanical Engineering

Dr. Justin Weibel

School of Mechanical Engineering

Approved by:

Dr. Nicole Key

To everyone who made this happen

ACKNOWLEDGMENTS

I have received a great deal of support over the last two years as I worked on this thesis. I would first like to thank my advisors Professor Amy Marconnet and Professor Fabio Semperlotti, for being great mentors and guiding me through this research. Their advice and insight helped me immensely as I continued my education and research at Purdue. I would also like to thank Professor Justin Weibel for being a part of the committee and offering advice, especially when I needed it in the first semester. My university experience became very blissful thanks to the support and advice given by these three amazing mentors.

I am also thankful for the guidance I received from Professor Xiulin Ruan and Dr. Giuseppe Romano, especially when I was learning to apply molecular dynamics techniques and Boltzmann transport equation solvers to my research. I would also like to thank my lab mates Albraa Alsaati, Zixin Xiong, and Ting-Wei Liu for always helping me figure out and learn new skills needed for my research. Their patience in reviewing my work and guiding me in tasks I was still learning was one of the reasons why I was able to finish this thesis. Though my work on phase change material experiments did not become a part of this thesis, the experience helped me learn multiple skills needed to develop myself as a thermal engineer. So, I am very thankful to Prahlad Kulkarni for building the experimental setup and everyone at Birck Nanotechnology Center for providing the resources needed for those experiments.

Finally, I would like to thank my parents Narayana Rao and Varalakshmi, for their unparalleled support all these years. In addition, I would also like to thank all my friends who stuck with me through this journey.

TABLE OF CONTENTS

LIST OF TABLES	8
LIST OF FIGURES	9
ABSTRACT	11
1 INTRODUCTION	13
1.1 Phononic Crystals and Applications	13
1.2 Phonons and Types of Phonon Transport	14
1.3 Lattice Thermal Conductivity Calculation Approaches	15
1.3.1 Molecular Dynamics Method	17
1.3.2 Boltzmann Transport Equation Solvers	18
Finite Volume BTE Solver with the Relaxation Time Approximation	18
Monte Carlo Method-based BTE solvers	19
Thermal Conductivity Integral: Callaway-Holland Model	20
1.4 Gaps in Current Literature	20
1.5 Objective of the Thesis	22
1.6 Overview of the Thesis	23
2 NON-EQUILIBRIUM MOLECULAR DYNAMICS	25
2.1 Introduction	25
2.2 NEMD Methodology	26
2.2.1 Algorithm	26
Material Crystal Structure Study	27
Definition of Simulation Domain	28
Initial System Relaxation	29
Heat Transfer Initiation	29
Thermal Conductivity Estimation	30
2.3 Implementation of Strain in the model	31
2.4 Closure	33

3	RELAXATION TIME APPROXIMATION BASED BTE SOLVER	34
3.1	Introduction	34
3.2	Boltzmann Transport Equation	35
3.2.1	General Form	35
3.2.2	Relaxation Time Approximation (RTA)	37
3.3	Software Solution Methodology	38
3.3.1	Simulation Domain and Boundary Conditions	38
3.3.2	Solution Framework	39
3.3.3	Modules in the Software	40
	Geometry Module	40
	Material Module	41
	RTA-BTE Solver Module	41
3.4	Implementation of Strain in the model and Closure	41
4	VARIANCE REDUCED MONTE CARLO METHOD FOR BTE	43
4.1	Introduction	43
4.2	MC Methods to Solve BTE - Approach	44
4.2.1	Simulation Domain Definition	44
4.2.2	Phonon Bundle Generation	46
4.2.3	Phonon Mobilization through Advection	47
4.2.4	Temperature Sampling	48
4.2.5	Phonon Internal Scattering	48
4.3	Calculation of Phonon Dispersion Relations	49
4.3.1	Continuum Mechanics based Phonon Dispersion Relations	49
4.4	Implementation of Strain in the Model	51
4.5	Closure	53
5	CALLAWAY-HOLLAND MODEL	54
5.1	Introduction	54
5.2	Governing Transport Equation - BTE	54
5.3	Callaway-Holland Analytical model	56

5.4	Implementation of Strain in the Model	57
5.5	Closure	58
6	RESULTS	59
6.1	Thermal Conductivity Estimation of Single Layer Graphene Lattice	59
6.1.1	Prediction and Validation of Thermal Conductivity from First Prin- ciple Calculations	59
6.1.2	Thermal Conductivity from Callaway-Holland Method	60
6.1.3	Thermal Conductivity from the Monte Carlo Method	62
6.1.4	Thermal conductivity from OpenBTE solver	63
6.1.5	Thermal Conductivity from Non-Equilibrium Molecular Dynamics . .	64
6.1.6	Comparison of Predicted Thermal Conductivity	66
6.2	Size Effects on the Thermal Conductivity of Single Layer Graphene	67
6.3	Thermal Conductivity for Lattices with Different Pore Geometries	68
6.3.1	Thermal Conductivity Prediction Results	69
6.4	Modeling the Effect of Strain on SLG PnC Thermal Conductivity	71
6.4.1	Methodology	71
6.4.2	Impact of Strain on Thermal Conductivity	71
6.4.3	Impact of Strain on Thermal Transport Anisotropy	73
6.4.4	Combined Effects of Lattice Size, Pore Geometry, and Heat Flow Paths	76
6.5	Closure	77
7	CONCLUSION	78
7.1	Conclusion	78
7.2	Contribution	79
7.3	Future Work	80
	REFERENCES	82

LIST OF TABLES

4.1	Calculated properties of single layer graphene using molecular mechanics calculations	50
6.1	Curve-fitted constants for the Callaway-Holland model for Single layer graphene with no pores	61
6.2	Computation time for a thermal conductivity prediction for each method	67
6.3	Estimated Thermal Conductivity values for Single Layer Graphene lattices (20nm x 20nm) with different pore geometries	69
6.4	Thermal conductivity under uniaxial strain of 6% for Single Layer Graphene lattices (20nm x 20nm) with different pore geometries (predicted using NEMD).	72
6.5	Thermal conductivity under uniaxial strain of 6% for Single Layer Graphene lattices (20nm x 20nm) with different pore geometries (predicted using Monte Carlo and Callaway-Holland models).	73
6.6	Estimated Thermal Anisotropy Deviations under uniaxial strain of 6% for Single Layer Graphene lattices (20nm x 20nm) with different pore geometries	74

LIST OF FIGURES

1.1	An overview of techniques used and effects described in this work.	23
2.1	A typical algorithm utilized by an NEMD solver to calculate thermal conductivity.	27
2.2	Schematic representation of graphene crystal structure.	28
2.3	Schematic of Graphene simulation domain with applied boundary conditions.	30
2.4	Schematic of two different simulation domains which are used to estimate thermal conductivity of single layer graphene in both zigzag and armchair directions (The red shaded areas denote hot regions, while the blue shaded area denotes the cold region).	32
2.5	Modified NEMD algorithm to model the effect of deformation(strain) on thermal conductivity.	33
3.1	A sample simulation domain used in OpenBTE along with the applied boundary conditions.	39
3.2	Software framework for OpenBTE solver (reproduced from [43]).	40
4.1	A typical algorithm followed by an MC-based BTE solver.	45
4.2	A sample lattice domain showing boundary conditions.	46
4.3	A sample lattice with mesh of appropriate element size.	51
4.4	A sample domain showing boundary conditions applied.	52
4.5	Figure showing Brillouin Zone (shaded area) in reciprocal space.	52
4.6	Algorithm implemented to obtain pre and post strain dispersion relations.	53
6.1	Validation of thermal conductivity of SLG calculated from AlmaBTE solver against Opto-thermal experimental data [91] and Tersoff-based NEMD solver output [92].	60
6.2	Calibration of thermal conductivity of SLG calculated using Callaway-Holland model against AlmaBTE values.	61
6.3	Thermal conductivity predictions at each time step in the VRMC simulation.	62
6.4	Comparison of thermal conductivity of SLG obtained using VRMC model against baseline data from AlmaBTE.	63
6.5	Heat Flux of SLG lattice predicted from OpenBTE solver.	63
6.6	Energy in eV transferred at hot and cold regions during each time step of the NEMD simulation.	64
6.7	Temperature distribution as a function of position within the simulation domain in the direction of heat flow.	65

6.8	Comparison of thermal conductivity predictions at 300 K for SLG sheet with no pores calculated with the experimental [91], [93] and theoretical [94] predictions.	66
6.9	A lattice with random pore geometry and the corresponding size effects on thermal conductivity.	68
6.10	Cumulative thermal conductivity of SLG as a function of phonon MFP from AlmaBTE.	68
6.11	Illustration of methods to predict thermal transport and which strain-dependent transport mechanisms are included.	72
6.12	Dominant heat flow paths (indicated by red arrows) based on heat flux distributions in each lattice calculated from the OpenBTE solver.	75

ABSTRACT

Understanding thermal transport across length scales lays the foundation to developing high-performance electronic devices. Although many experiments and models of the past few decades have explored the physics of heat transfer at nanoscale, there are still open questions regarding the impact of periodic nanostructuring and coherent phonon effects, as well as the interaction of strain and thermal transport. Thermomechanical effects, as well as strains applied in flexible electronic devices, impact the thermal transport. In the simplest kinetic theory models, thermal conductivity is proportional to the phonon group velocity, heat capacity, and scattering times. Periodic porous nanostructures impact the phonon dispersion relationship (group velocity) and the boundaries of the pores increase the scattering times. Strain, on the other hand, affects the crystal structure of the lattice and slightly increases the thermal conductivity of the material under compression. Intriguingly, applying strain combined with the periodic porous structures is expected to influence both the dispersion relation and scattering rates and yield the ability to tune thermal transport actively. But often these interrelated effects are simplified in models.

This work evaluates the combination of structure and strain on thermal conductivity by revisiting some of the essential methods used to predict thermal transport for a single layer of graphene with a periodic porous lattice structure with and without applied strain. First, we use the highest fidelity method of Non-Equilibrium Molecular Dynamics (NEMD) simulations to estimate the thermal conductivity which considers the impact of the lattice structure, strain state, and phononic band structure together. Next, the impact of the geometry of the slots within the lattice is interrogated with Boltzmann Transport Equation (BTE) models under a Relaxation Time Approximation. A Monte Carlo based Boltzmann Transport Equation (BTE) solver is also used to estimate the thermal conductivity of phononic crystals with varying pore geometry. Dispersion relations calculated from continuum mechanics are used as input here. This method which utilizes a simplified pore geometry only partially accounts for the effects of scattering on the pore boundaries. Finally, a continuum level model is also used to predict the thermal conductivity and its variations under applied strain. As acoustic

phonon branches tend to carry the most heat within the lattice, these continuum models and other simple kinetic theories only consider their group velocities to estimate their impact on phonon thermal conductivity. As such, they do not take into account the details of phonon transport across all wavelengths.

By comparing the results from these different methods, each of which has different assumptions and simplifications, the current work aims to understand the effects of changes to the dispersion relationship based on strain and the periodic nanostructures on the thermal conductivity. We evaluate the accuracy of the kinetic theory, ray tracing, and BTE models in comparison to the MD results to offer a perspective of the reliability of each method of thermal conductivity estimation. In addition, the effect of strain on each phononic crystal with different pore geometry is also predicted in terms of change to their in-plane thermal anisotropy values. To summarize, this deeper understanding of the nanoscale thermal transport and the interrelated effects of geometry, strain, and phonon band structure on thermal conductivity can aid in developing lattices specifically designed to achieve the required dynamic thermal response for future nano-scale thermoelectric applications.

1. INTRODUCTION

The electronics industry continues to grow while the thermal requirements for applications have been getting more challenging. The demand for miniaturization and new transistor technologies led to the need to understand low-dimensional materials. Developing application-specific lattice designs may enable the control of thermal properties. For example, the ability to direct heat flow and manipulate thermal conductivity in electronics applications could enable more reliable devices by routing heat around delicate components. This has driven the scientific community towards understanding and controlling thermal transport in materials. One class of materials that has been developed to tune mechanical and thermal properties are called phononic crystals (PnCs). These are metamaterials, often consisting of thin layers, with engineered pore geometry, vacancies and inclusions designed for a particular application. Much of the current work aims to contribute towards understanding and modeling such materials for thermoelectric applications [1], [2]. But here, these systems are evaluated for the control of thermal transport.

1.1 Phononic Crystals and Applications

Phononic crystals are metamaterials designed to tune the propagation of sound and heat within them. Since the propagation of heat and sound depends on the properties of the energy carriers within the PnCs, the tuning is mostly achieved by relying on the effects on these properties due to the different pore geometries and lattice configurations. Some of the common methods explored currently are by introducing vacancies and impurities within the PnCs [3], varying pore shape [4] and material layer thicknesses [5], in addition to developing composite PnCs [6]. This tunability of properties in these materials presents an opportunity for electronics thermal management applications which need nanoscale materials for thermal shielding or heat flow deflection. In cases where high-energy density hot spots are common, the inclusion of phononic crystals to tune the thermal behavior has been studied both theoretically [4]–[7] and experimentally [8], [9]. Hole and pillar based phononic crystals have been studied to investigate their applicability to electronics [1], [4], [8], [10], [11], with pillar based crystals being favored as they do not significantly affect the overall electrical conduc-

tivity. Thermally shielding or cloaking using phononic crystals has also been explored to ensure heat sensitive devices within the the electronics do not experience high temperatures during operation [12]–[14]. While some studies focused on developing phononic crystals for these application, others have explored different material options for the same applications. Some of the materials investigated are Graphene [4], [9], [15], Silicon [1], [11], [16], [17], Boron Nitride [18], [19], Phosphorene [20]–[22] and Molybdenum Disulphide [23]–[25]. The phonon band structure of materials like silicon are nearly isotropic, while that of Graphene and Phosphorene are anisotropic. Each material also has different electronic properties. Especially for thermoelectric materials, the ability to reduce the thermal conductivity without disturbing the electrical conductivity is needed. In such cases, phononic crystals can greatly improve the overall thermoelectric performance [26], [27]. The demand from these applications combined with the complex physics involved with these phononic crystals is what drives the need for more research towards these materials.

1.2 Phonons and Types of Phonon Transport

In phononic crystals, heat is carried by quantized modes of vibrations called phonons. These phonons are modeled with both particle and wave-like behavior to predict the overall energy transfer, thermal conductivity, and dispersion relations. Phonons can transport in different wavemodes which are determined by the material dispersion relationships and the corresponding density of states. Phonons can carry heat in different ways depending on how the geometry scale compares to the mean free path (MFP). When the length scale of the system becomes comparable to the phonon wavelengths and mean free paths, the physics of predicting thermal conductivity becomes complex due to the interaction of phonons with each other, domain boundaries, interfaces, and impurities, as well as changes to the allowed modes due to the geometry.

The transport modes based on the lattice constant and phonon mean free path are compared using a parameter called Knudsen number, Kn . The Knudsen number is the ratio of phonon mean free path to a characteristic length scale (such as lattice constant), $Kn = \frac{\Lambda}{L}$, where Λ is the phonon mean free path and L is the characteristic length of the phononic

crystal considered. Depending on the range of the Knudsen number, three different phonon transport regimes can be defined. They are as follows:

1. **Diffusive Transport:** When phonon mean free path is significantly smaller than the characteristic length scale of the lattice (*i.e.*, when $Kn \ll 1$), the phonon transport is dominated by collisions, and the heat transfer is diffusive. This applies at the macroscale where Fourier’s law can be used to accurately model the heat transfer within the material.
2. **Ballistic Transport:** On the other hand, when the phonon mean free path is very large compared to the characteristic length of the lattice (*i.e.*, when $Kn \gg 1$), the phonons directly transmit the heat without interacting with any of the other phonons or boundaries. This absence of internal scattering where carrier-carrier interactions can be completely neglected, is the ballistic phonon transport regime and phonon group velocities alone can be used to model the heat flow.
3. **Transitional Region:** Finally, when the phonon mean free path and the characteristic length are comparable (*i.e.*, when $0.1 < Kn < 10$), the overall phonon transport is a combination of diffusive and ballistic transport where carrier interactions are significant. Here, modeling at the atomic scale is needed to account for phonon transport within the region making this the most complex region to simulate. Several techniques have been developed to solve for phonon transport within this region including molecular dynamics models based on simulating the atomic motion.

1.3 Lattice Thermal Conductivity Calculation Approaches

Phonon transport modeling is critical for understanding heat transfer in phononic crystals. As such, multiple techniques have been proposed to model phonons based on various set of assumptions and considerations. Depending on the available computational power and time, different methods can model the heat transfer within the phononic crystals. Approaches range from high fidelity models computing atom positions and interatomic potentials to lower fidelity approximate continuum models. For bulk materials, certain assumptions like uniform

properties and isotropic band structures are typically assumed. These assumptions make the systems simpler to model. But care needs to be taken to ensure that the accuracy of the model is not affected too much by the assumptions. In this work, four different phonon modeling approaches, falling into two main categories, are used:

1. **Molecular Dynamics (MD) Methods:** This is the most detailed thermal transport model as every feature starting from geometry to phonon flow is simulated using atomic vibrations within the lattice. Here, the lattice crystal structure is obtained using first principle calculations or experiments and interatomic potentials are applied to simulate energy transfer. Depending on the energy formulation and boundary conditions, MD simulations are categorized into multiple types. Though these MD models are very accurate, they are extremely computationally expensive.
2. **Boltzmann Transport Equation (BTE) Solvers:** As an alternative to computationally expensive models, BTE solvers utilize the wave-particle duality of phonons to simulate their transport within the PnCs. The Boltzmann transport equation is based on conservation of the energy carrying “particles” within a medium. It applies to both electrons and phonons and is used to predict the corresponding conductivity values. This equation is used together with material and geometry based assumptions to predict the overall thermal transport in a PnC.
 - **BTE Solver - Finite Volume Approach:** One approach to solve the BTE involves discretizing the domain and applying the particle conservation equation using a finite volume approach. Some of the most common assumptions used are that the band structure is isotropic, the material is 2D, and the relaxation time approximation (which will be discussed in detail in Chapters 3) applies. These methods utilize phonon dispersion relations as input to predict the phonon transport within the PnC for any given pore geometry.
 - **BTE Solver - Monte Carlo Methods:** Another method to solve the BTE leverages the Monte Carlo approach to predict phonon thermal conductivity based on their particle-like behavior by randomly placing phonon packets in the struc-

ture and simulating their motion and interaction. This requires inputs from the band structure including the phonon group velocities obtained either through first principle calculations or simplified continuum models and known internal scattering phenomenon. A reasonably small time step is chosen and all the accounted effects within the PnC are calculated. This simulation continues until the conductivity predictions converge. Due to the need to simulate large number of phonon packets for many number of time steps to reach convergence, MC methods are usually very computationally expensive too. So, these methods use different assumptions to simplify the model and reduce the computation time. These will be described in detail in Chapter 4.

- **Simplified BTE - Thermal Conductivity Integral Approach:** The BTE or kinetic theory can be used to derive a simplified equation to predict thermal conductivity based on the band structure and scattering mechanisms within a system. This approach, commonly referred to as a Callaway-Holland Model [28]–[30], is very computationally efficient, but omits details of the geometry as scattering at boundaries is typically included based on a characteristic length scale. Similar to the Monte Carlo solvers, it requires inputs of the dispersion relationship and scattering mechanisms, and often many assumptions are required including the relaxation time approximation.

1.3.1 Molecular Dynamics Method

Molecular dynamics methods predict the phonon transport based on the understanding that phonons are quantized lattice vibrations carrying energy[31]–[34]. Here, the material is modeled at the atomic level with vibrations predicted based on the interatomic structure. The bonds, bond lengths and interatomic potentials are obtained using first principle calculations or experimental techniques like spectroscopy. The vibrational modes are calculated to estimate the energy transfer within the lattice. This method has high fidelity but is computationally expensive. There are multiple types of molecular dynamics methods, depending on the type of heat source and method to estimate energy transport including Equilibrium

Molecular Dynamics (EMD)[35], [36], Non-Equilibrium Molecular Dynamics (NEMD)[37], [38], and Reverse Non-Equilibrium Molecular Dynamics (RNEMD)[39], [40]. Molecular dynamics models require knowledge of the interatomic potentials between neighboring atoms and these vary depending on the material. These first principle based calculations should lead to the most accurate predictions of phonon thermal conductivity, but their extremely high computational cost makes them challenging to apply to multiple PnC configurations. This work uses NEMD to model phonon transport for selected geometry. A more detailed description on this method is discussed in Chapter 2.

1.3.2 Boltzmann Transport Equation Solvers

Since phonons can be considered as particles of "phonon gas" due to their particle-like nature, a conservation of number of particles can be used as the fundamental equation governing the phonon flow. This equation is called the Boltzmann Transport Equation (BTE), which describes the conservation of particles like phonons and electrons in phase-space. Applying this to phonons involves solving for both diffusive as well as collision based phonon population change with time. A typical formulation of this BTE is as in the equation 1.1:

$$\left(\frac{\partial n}{\partial t}\right) + \mathbf{v}_g \cdot (\nabla_r n) = \left(\frac{\partial n}{\partial t}\right)_{scattering}, \quad (1.1)$$

where n is the energy carrier (phonon) population distribution and v_g is the group velocity of phonon wave modes of interest. Different methods to estimate these terms, specifically the scattering term, causes differences between each solver.

Finite Volume BTE Solver with the Relaxation Time Approximation

Due to the complexity in phonon scattering within a lattice, numerous approaches are chosen to simplify and predict phonon scattering effects. One such approximation is the re-

laxation time approximation (RTA), which assumes that the deviation in phonon population from the equilibrium population due to scattering is linear with time:

$$\left(\frac{\partial n}{\partial t}\right)_{\text{scattering}} = -\frac{(n - n_0)}{\tau}, \quad (1.2)$$

where τ is the relaxation time due to the internal phonon scattering processes and n_0 is the equilibrium phonon population distribution at a given temperature T defined by Bose-Einstein distribution. This approximation simplifies the BTE equation to a linear form, which can be discretized using a finite volume approach and applied to a PnC domain of interest. The discretization technique and the time step are chosen depending on the type of geometry involved. These solvers also utilize dispersion relations as input to predict the lattice thermal conductivity[41], [42]. One such solver used in this work is OpenBTE [43]. It is an open-source solver which uses linearized BTE as the governing equation. This deterministic solver applies BTE to all the three directions but assumes an isotropic and uniform material to simplify the model as needed. A more detailed description on the method, its advantages and disadvantages are discussed in Chapter 3.

Monte Carlo Method-based BTE solvers

While deterministic solvers are a good approach to utilize for simple cases, methods based on probability and sampling like Monte Carlo methods become helpful to simulate multiple complex phonon interactions at once. While modeling scattering and phonon-phonon collisions in other methods requires defining many effective terms based on the wave nature of phonons, Monte Carlo methods use the particle nature to model every phonon or group of phonons as a bunch traveling together and colliding with boundaries, interfaces and other phonons[44], [45]. Each phonon is randomly assigned a position, a wave mode and direction in the beginning of the simulation, and after each time step, they travel with the group velocity extracted from the phonon dispersion relations. These dispersion relations, which are used as input to this solver, are obtained either through first principle calculations or simplified continuum models based on structural mechanics. At each time step, the

phonons are allowed to traverse and interact with other phonons and boundaries. These phonon collisions, their new velocities and the resultant conductivity are calculated at each time step before continuing to the next time step. To sample the thermal conductivity accurately, a large number of phonons have to be simulated this way thus increasing the technique's overall computational cost. On the other hand, since this is not a mesh or element dependent simulation, the computational cost only increases linearly with lattice scale making this a suitable approach for slightly larger simulation domains.

Thermal Conductivity Integral: Callaway-Holland Model

Callaway-Holland model is based on a simplified analytical solution to the BTE developed to predict phonon transport within bulk materials and thin layers[28]–[30]. It generally assumes a uniform, isotropic material with only the first three acoustic wave modes contributing to the total thermal transport. The relaxation time approximation, used in this model, assumes that the rate of change of phonon population due to scattering is linear. The phonon dispersion relations from first principle calculations or continuum models are used to extract group velocities, specific heat, relaxation times and are then used to calculate the thermal conductivity as in the equation 1.3:

$$k = \frac{1}{6\pi^2} \sum_i \int_q (C)(v)^2(\tau)q^2 dq, \quad (1.3)$$

where k , i , q , C , v are thermal conductivity, wave mode branch index, phonon wave number, specific heat and group velocity of each phonon respectively. This is one of the simplest phonon transport models as it does not use complex functions to define internal scattering. Thus, the computation time is the least out of all explored methods in this work. A detailed description of this method is presented in Chapter 5.

1.4 Gaps in Current Literature

Despite the diverse and detailed research on modeling phonon transport, there are still open questions related to thermal transport in PnCs. Though some works have attempted to

report experimental data on PnCs [46], [47], the predicted ideal lattice sizes are on the order of a few nanometers. Thus, the PnC fabrication and experimentation is often at larger length scales thus limiting the comparison to models. In addition to this, the multiple scattering phenomenon and numerous wave modes make it complex to model the phonon flow. Though a few works have presented some level of understanding of phonon flow in simple lattices [48]–[50] and the effect of thickness on the phonon flow [51], [52], there are still gaps in knowledge especially on a few PnCs with complex pore geometries and interface scattering. On that account, a few major voids in current research include:

- **Accuracy of the phonon transport model**

Even though multiple models and methods have been proposed to estimate phonon transport in PnCs [53]–[56], a model that balances accuracy and computational expense is still missing. While this is partly due to the complex phonon behavior, it is also due to the incomplete understanding of internal scattering processes. Therefore more work towards understanding internal scattering is needed to head towards developing an accurate and fast phonon transport simulation.

- **Effect of individual phonon properties on the overall heat flow**

While there is some understanding of phonon behavior including their fundamental particle nature [57], [58] and wave nature [59], [60], as well as the dispersion relations [61], [62], a detailed understanding of effect of each different phonon property on the overall PnC thermal behavior is missing. This knowledge is a necessary part of designing PnCs for specialized applications and hence, a significant part of phonon research should be steered in this direction.

- **Experimental investigation of nanoscale PnCs**

Experimental investigations form the baseline data for model validation. With PnCs, the experiments to perform are complex due to their small scale and non-linear thermal behavior. This level of complexity and the corresponding lack of experimental data needs to be resolved to effectively validate any future transport models or measure properties of newly developed PnC composites.

- **Effect of external actuation like strain on phonon behavior**

While phonon transport itself is complex, the effect of external force or strain acting on the PnC can lead to effects which are not completely understood at this point. Though some work on the effect of strain on PnCS is already performed using various existing models [63] and experiments [64], these do not report completely the causes behind the results or the phenomena taking place thus indicating a lack of understanding in this area too.

1.5 Objective of the Thesis

This thesis aims to address open questions regarding the phonon transport in PnCs and the effect of different phonon parameters and strain on the overall thermal transport behavior of the PnC. The current work first investigates the accuracy of the different thermal modeling approaches for phonon transport by evaluating single layer graphene (SLG) with numerous types of pore structures that form lattices. SLG was chosen specifically as it is a single layer material with small lattice size enabling easier usage of computationally heavy MD methods. In addition to this, SLG's molecular structure and equivalent elastic properties are also widely available. Silicon is also a good option for the test material as its fabrication in an experimental environment is relatively easier. But applying MD methods on Silicon PnCs is computationally too expensive for the current resources available. Thus SLG is chosen as the test material to study phonon thermal transport in this thesis.

Initially, we investigate the size effects and phonon scattering at pore boundaries in fixed geometries using the different modeling approaches. An overview of different methods used in this work and effects each method consider are shown in the Figure 1.1. Understanding phonon thermal transport requires addressing different effects starting from the dispersion relations, wave modes and group velocities to scattering at nanopore boundaries and interfaces. These effects originating from different phonon transport features like pore geometry and dispersion relations are laid out in the Figure 1.1, and the corresponding methods with a capability to predict each of them is shown beside. These methods are used in combination

to possibly separate and understand the various transport features of phonons in single layer graphene.

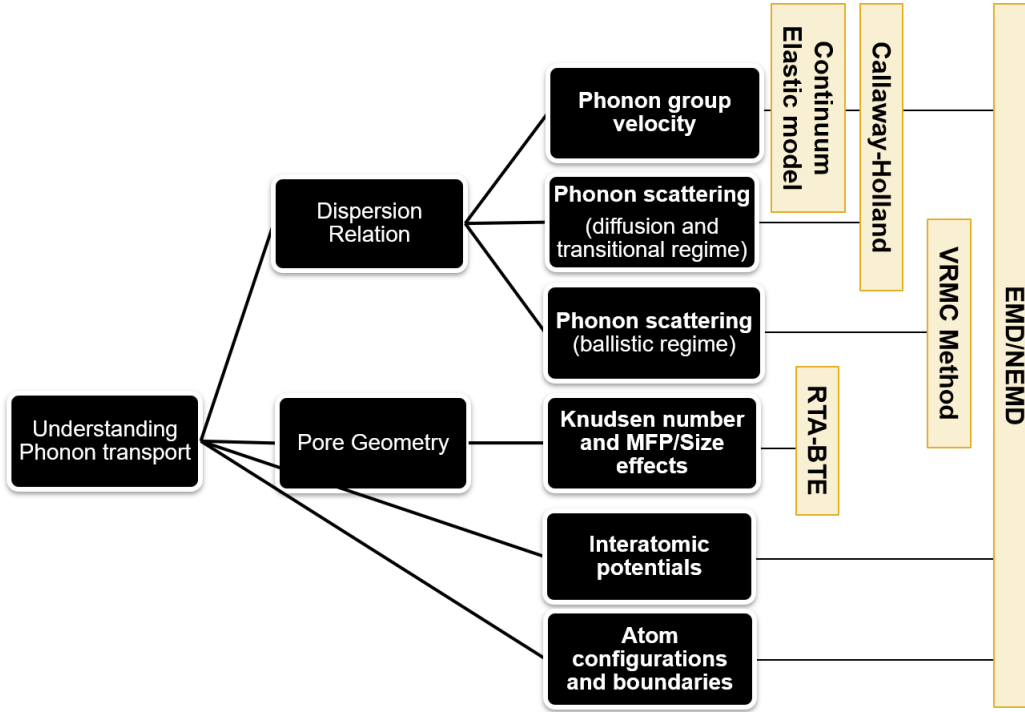


Figure 1.1. An overview of techniques used and effects described in this work.

In addition to controlling the pore geometry, the impact of strain on the PnCs is investigated based on the approach discussed to identify the features affecting the phonon transport with an applied strain. Since each method introduced takes into account only some of the scattering mechanisms, the results from multiple models are utilized to identify directions to design a lattice highly sensitive to external strain. This approach and the corresponding inferences from each technique are described in detail in Chapter 6.

1.6 Overview of the Thesis

The current work first discusses different techniques to model the phonon transport starting with the high fidelity NEMD model in Chapter 2 followed by Boltzmann transport equation solvers in Chapter 3. It is then followed by variance reduced Monte Carlo model and Callaway-Holland models in chapters 4-5. Finally, the results from each technique are

discussed in Chapter 6 followed by addressing the contribution and future directions in Chapter 7.

2. NON-EQUILIBRIUM MOLECULAR DYNAMICS

2.1 Introduction

With the need for more accurate phonon transport studies, methods like molecular dynamics were explored which are computationally very expensive but accepted widely as one of the most accurate material analyzing tools. As such, these MD methods have been applied to phononic nanocrystals as well to calculate phonon properties like dispersion plots and relaxation times [31], [32]. MD methods have also been applied to predict heat fluxes and thermal conductivity values of PnCs [33], [34]. Since Molecular Dynamics involves studying time evolution of each specific atom and its interaction with neighbours, the accuracy of the model is very high as long as the interatomic interactions (potential) are defined well. But this advantage in accuracy comes at a high price of extreme computational expense. In addition to this, the domain size that can be simulated is very less thus leading to size effects coming into play during the simulation. This necessitates careful planning of the simulations.

Molecular dynamics is, simply put, an application of Newton's second law of motion at classical level to a system of atoms. Thus, if a lattice or metamaterial needs to be analyzed by Molecular Dynamics(MD), its atomic structure has to be known in advance along with their bond lengths, angles and interatomic interaction. In a simple domain of atoms under MD study, the interatomic force is calculated from interatomic potential function. There are multiple types of potentials in application currently like Tersoff potential [65], [66]; Weber potential [67], [68]; and other reactive potentials [69], [70]. Using these and applying boundary conditions on different atomic systems, their equivalent properties are estimated. In this chapter, the molecular dynamics technique, its different variants and finally its application to phononic nanocrystal analysis is discussed.

2.2 NEMD Methodology

Molecular dynamics simulations runs on the application of second law of motion. If a system of atoms is considered, this application of second law gives the following equation:

$$M \frac{d^2 \mathbf{r}_i}{dt^2} = \sum_{j, j \neq i}^N \mathbf{F}_{i,j} \quad (2.1)$$

where M is the mass of each atom, N is the total number of atoms, while \mathbf{r} and \mathbf{F} are position and interatomic potential of each atom. Here, the force of interaction $F_{i,j}$ is obtained by deriving interatomic potential as:

$$\mathbf{F}_{i,j} = \frac{\partial \phi_{i,j}}{\partial \mathbf{r}} \quad (2.2)$$

These equations form the basis of the Molecular dynamics methods as these forces and atom movements(vibrations) are used later to calculate dispersion relations and other similar properties accurately. There are two major types of Molecular Dynamics techniques - Equilibrium Molecular Dynamics (EMD) [35], [36], and Non-Equilibrium Molecular Dynamics (NEMD) [37], [38]. There are also recently developed techniques like Reverse Non-Equilibrium Molecular Dynamics (RNEMD) [39], [40]. The key difference between all of these methods is how the energy source is treated within the atomic system. In EMD, Green-Kubo formulation[71], [72] is used and the temperature is kept constant throughout the simulation, while in NEMD, a temperature gradient is applied on the lattice and thermal conductivity is calculated from the obtained heat flux using Fourier's law. In RNEMD, the cause and effect are reversed as heat flux is imposed on the system initially and the corresponding temperature gradient is calculated to predict the thermal conductivity. In this thesis, NEMD is used to predict thermal conductivity of single layer graphene PnCs with different pore geometries.

2.2.1 Algorithm

Since the MD technique is at classical level involving force calculations and energy balances, there are multiple algorithms followed to estimate thermal conductivity. This is what

led to the development of new techniques like RNEMD. A typical algorithm used in an NEMD solver to estimate thermal conductivity of a given crystal structure is as shown in the Figure 2.1. The technique involves following substeps in series:

1. Crystal structure study
2. Definition of simulation domain
3. Initial system relaxation/equilibrium
4. Heat transfer initiation
5. Temperature gradient and thermal conductivity estimation

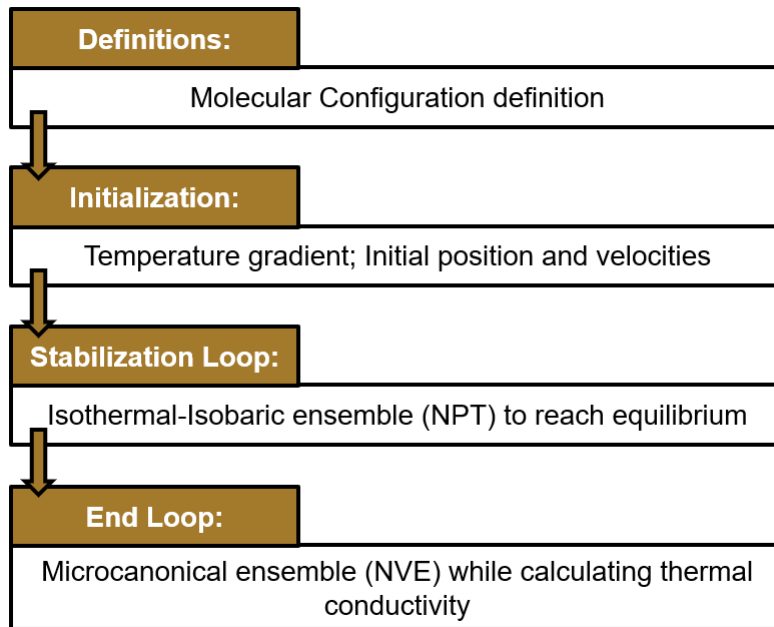


Figure 2.1. A typical algorithm utilized by an NEMD solver to calculate thermal conductivity.

Material Crystal Structure Study

While NEMD offers a very accurate route to analyzing phonon transport, one of the input terms needed for the technique is the atomic configuration. Since atom positions are

used directly to calculate interatomic potentials, the bond length, bond angle and other such parameters directly effect the simulation. Especially when it comes to anisotropic materials like graphene, the atom positions have to be accurately calculated. So, many researchers utilize the already experimentally measured atom positions. For this study, the graphene structure from Franz et al. [73] is used to calculate the atom positions in the simulation domain. The schematic representation of unit cell of single layer graphene is as shown in the Figure 2.2. Here, the horizontal direction is armchair direction while the vertical one is zigzag direction.

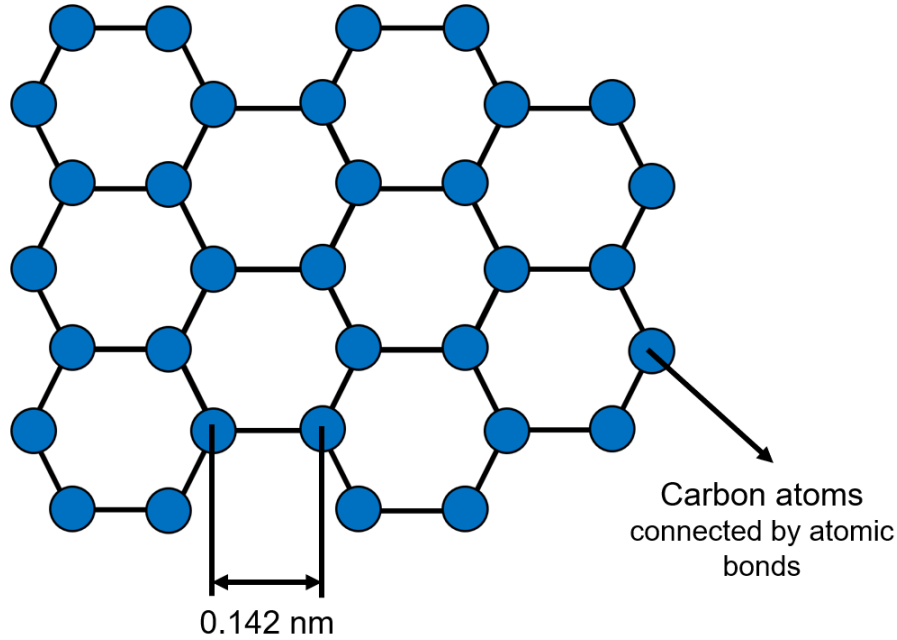


Figure 2.2. Schematic representation of graphene crystal structure.

Definition of Simulation Domain

As seen in the Figure 2.2, the lattice constant is about 0.142 nm with the inter-layer distance between graphene layers being around 0.335 nm. These distances are used to calculate atom positions to fill up a total space of a 40 nm x 10 nm simulation domain. This results in a total of around 16656 atoms within the domain. Each of these atom positions are

calculated accurately using the bond lengths from Franz et al. [73], and a Tersoff potential function is used on the system. An equilibrium temperature of 300 K and a timestep of 0.5 fs are chosen for the current study.

Initial System Relaxation

With the simulation domain ready as input, the molecular dynamics method can now be performed, and that is done here using LAMMPS solver [74]. Though the atom positions are carefully calculated using the bond properties from Franz et al. [73], it is still essential that the system is allowed to relax before any energy transfer. This is to ensure that the atoms reach their equilibrium positions and are stabilized before any external action can be applied on the system. This equilibrium is achieved by enforcing an Isothermal-Isobaric ensemble (a constant atom number, pressure and temperature process - NPT) for about 1000000 time steps. This constant pressure and temperature process allows the atoms to stretch or compress to any equilibrium dimension freely.

Heat Transfer Initiation

Once this step is completed, a temperature gradient of 10-20 K is applied on the system under NVE ensemble to initiate heat transfer. A Microcanonical ensemble (constant atom number, volume and energy - NVE) ensemble makes sure no energy is lost and geometry (shape) of the simulation domain stays intact. The boundary conditions applied on the simulation domain during this process are as shown in the Figure 2.3. The left and right end strips of atoms are assigned high temperatures to be Hot regions (shown in red), and the center strip of atoms are assigned low temperature to be Cold region (shown in blue).

It is made sure that the applied temperature gradient is along the length direction. This temperature gradient causes heat flow along the length direction as well. Periodic boundary conditions are applied at both X and Y boundaries. And for the overall (time-averaged) heat flow, Fourier's law of heat conduction can be utilized as follows.

$$\langle Q \rangle = -k \langle \nabla T \rangle \quad (2.3)$$

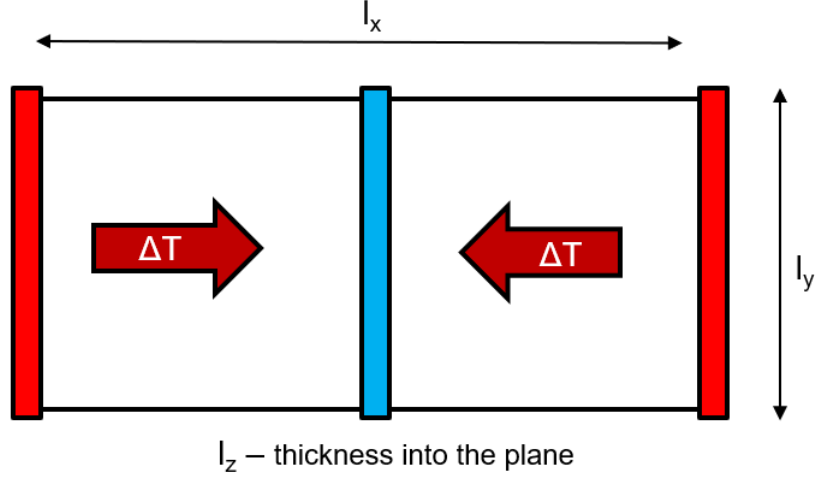


Figure 2.3. Schematic of Graphene simulation domain with applied boundary conditions.

where Q and ΔT are the heat flux and temperature gradient within the simulation domain while k is the thermal conductivity. Also, $\langle \rangle$ denotes the time-averaged quantities here.

Thermal Conductivity Estimation

After the temperature gradient is applied for enough number of time steps, say 40000, a time average of the temperatures and energies is calculated using the following method. The energy exchanged between the hottest and coldest atoms in the Hot region is calculated as ΔE . This exchanged energy is used to estimate the time-averaged heat flux within the system as follows:

$$\langle Q \rangle = -\frac{\langle \Delta E \rangle}{2A\Delta t}, \quad (2.4)$$

where A and Δt are the area of cross section of the Graphene domain and the simulation time step respectively. The temperature profile is also calculated by first splitting the domain into chosen number of parts in the direction of heat flow, say 50. An energy balance between the potential and kinetic energy is then used as follows:

$$N_i k_B T_i = \frac{1}{3} \sum_{j=1}^{N_i} m_j v_j^2, \quad (2.5)$$

where N_i and T_i are the number of atoms and their temperature in the part i of the domain while m_j and v_j are the mass and velocity values of each atom in that part. This equation, when simplified, provides the temperature profile, T_i as a function of kinetic energy of the internal atoms. Now, omitting the data near hot and cold region to avoid edge effects, the interior temperature points are chosen and a linear fit is used to obtain the temperature gradient in the direction of heat flow ($\frac{\partial T}{\partial x}$). This, along with the earlier calculated heat flux, is used to calculate the thermal conductivity in the direction of heat flow as the ratio of heat flux to temperature gradient which results in the following equation:

$$k = \frac{\langle \Delta E \rangle}{2A\Delta t \left(\frac{\partial T}{\partial x} \right)}. \quad (2.6)$$

The same approach can be applied to the other in plane direction by modifying the geometry of the simulation domain (see Figure 2.4). The longest side of the simulation domain should always be in the direction of heat flow to accommodate enough room to assign two hot and one cold regions. The configuration on the left side in the Figure 2.4 can be used to estimate the thermal conductivity in the armchair direction while the configuration on the right can be used to estimate the same in the zigzag direction.

2.3 Implementation of Strain in the model

To model the effect of strain on the phononic crystal thermal conductivity, the simulation domain has to undergo deformation before the temperature gradient can be applied. This necessitates a slight change in the NEMD algorithm presented in the Figure 2.1. The new algorithm which accounts for effect of strain on the simulation domain is shown in the Figure 2.5. Here are the substeps in the new algorithm:

1. Crystal structure study
2. Definition of Simulation domain
3. Initial system relaxation/equilibrium
4. Simulation domain deformation

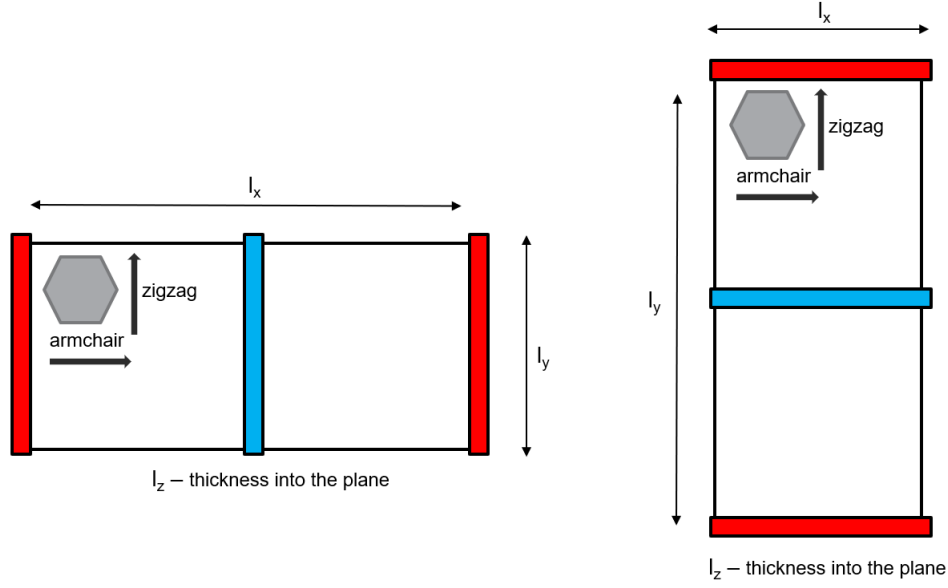


Figure 2.4. Schematic of two different simulation domains which are used to estimate thermal conductivity of single layer graphene in both zigzag and armchair directions (The red shaded areas denote hot regions, while the blue shaded area denotes the cold region).

5. Heat transfer initiation
6. Temperature gradient and thermal conductivity estimation

The biggest difference between the new algorithm and the old one, as seen from the Figure 2.5 in contrast to the Figure 2.1, is that a new deformation process under Canonical ensemble is enforced on the simulation domain. During this deformation process, the total strain is applied over a selected number of time steps under a constant strain rate. The Canonical ensemble (constant atom number, volume and temperature - NVT) allows the strain at each time step to not revert back to original by enforcing a constant volume condition. Once the strain application is complete, the system is let to relax again before the NEMD solver proceeds to apply the temperature gradient under an NVE ensemble. The rest of the method including the calculations follow a similar procedure as seen in the previous section for the unstrained single layer graphene case. With the strained case too, in order to obtain the

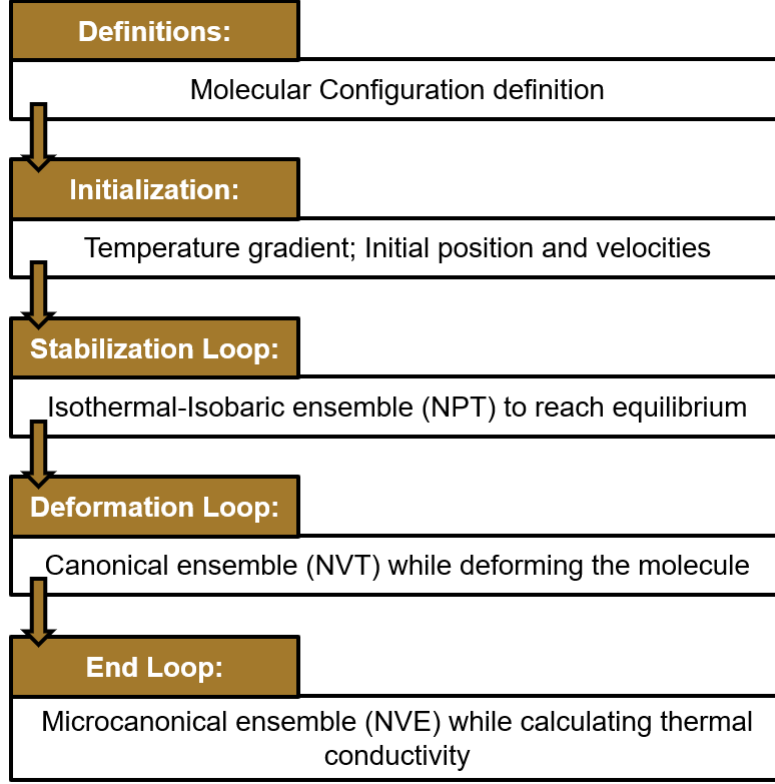


Figure 2.5. Modified NEMD algorithm to model the effect of deformation(strain) on thermal conductivity.

effect of strain on thermal conductivity in both zigzag and armchair directions, the simulation domain has to be modified again as shown in the Figure 2.4.

2.4 Closure

With the effect of strain included in the analysis, the thermal conductivity predictions calculated with NEMD before and after strain for different lattice geometries are reported in Chapter 6. In addition, the effect of strain on the thermal anisotropy is also studied. While the MD simulations can account for the detailed physics of strain on heat transfer, it is computationally expensive. Thus we consider other approaches of calculating thermal conductivity in the following chapters.

3. RELAXATION TIME APPROXIMATION BASED BTE SOLVER

3.1 Introduction

Modeling phonon transport within a material is complex due to their ballistic and diffusive nature. Dislocations, interfaces and other material configurations only add to the complexity of the modeling. The Boltzmann Transport equation is considered widely as the fundamental equation governing phonon transport in metamaterials, and thus becomes a part of any framework or algorithm solving for phonon transport. While many researchers have used traditional approaches like Callaway-Holland method [28]–[30] to estimate thermal conductivity, more recent techniques utilize a combination of first principles and density functional theory as inputs to BTE solvers[75], [76]. Based on these methods, researchers have utilized Python as a framework to devise solvers for the steady state BTE. One of the first solvers designed this way was ShengBTE [41] which is primarily made to solve thermal transport for bulk materials and nanowires. It solves the Boltzmann Transport Equation by using force constants obtained from fundamental first principles. Other solvers include FourPhonons [77] which solves the BTE for four phonon scattering, and Phono3Py [78] solver which solves BTE under relaxation time approximation. Another popular solver named AlmaBTE [42] solves for dispersion plots and thermal conductivity among other material properties in bulk materials, nanowires, thin films and superlattices using first principle calculations and solving BTE. There are other solver packages too like PhonTs [79] and ALAMODE [80] which solve for phonon transport. While most of these solvers which are designed for simpler geometries use deterministic solvers, the solvers which work on complex geometries use Monte Carlo methods.

The solver considered here, OpenBTE, developed by Romano et al. [43], solves the first principles and Boltzmann transport equation in three dimensions to solve for temperature, heat flux, and thermal conductivity for thin films and materials of complex geometry by using the bulk cumulative thermal properties as input. While the solver is still in development, it has been utilized and validated experimentally for silicon thin films within the range of 100nm [81].

3.2 Boltzmann Transport Equation

Heat transport in phononic crystals can be modeled as transport of energy packets (or particles). Following classical theory, phonon transport can be modeled as flow of particles and their conservation at steady state is a starting point to analyze their flow. This particular assumption becomes valid as long as the coherence effects in phonon transport can be neglected (*i.e* the quantum wave effects are not as important to the overall phonon flow). Under these set of assumptions and considerations, the conservation of number of particles or phonons at steady state is derived and called the Boltzmann transport equation. But when the characteristic length of the lattice system is smaller than the wavelength of phonons, the wave effects become very essential as the wave interference cannot be neglected. This leads the particle-based theory to fail and thus the BTE too. So, the Knudsen number helps identify the applicability of BTE (*i.e* when $Kn \gg 1$), the phonon transport is more ballistic and BTE is not very accurate. It can also be proved that BTE reduces to the standard Fourier law of heat conduction in the case of collision dominated heat flow (*i.e* at continuum limit, $Kn \ll 1$).

3.2.1 General Form

Now, if function ‘ f ’ defines the probability distribution to find a phonon, the Boltzmann transport equation indicates that there is no change in this probability distribution function in the material at steady state. So, the general form of BTE is as follows:

$$\left(\frac{\partial f}{\partial t}\right) = \left(\frac{\partial f}{\partial t}\right)_{diffusion} + \left(\frac{\partial f}{\partial t}\right)_{fields} + \left(\frac{\partial f}{\partial t}\right)_{collisions} \quad (3.1)$$

where $f(\mathbf{r}, \mathbf{k}, t)$ is the phonon probability distribution, a function in three dimensional space vector, \mathbf{r} , time t , and phonon wave vector, \mathbf{k} . Now, for the diffusion process, we are aware that the the rate of change with respect to time can be written in terms of velocity and rate with respect to position.

$$\left(\frac{\partial f}{\partial t}\right)_{diffusion} = -\mathbf{v} \cdot (\nabla_{\mathbf{r}} f) \quad (3.2)$$

where \mathbf{v} is the particle velocity of phonon, given by $\frac{\partial \mathbf{r}}{\partial t}$. Similarly for the rate under external fields, the term can be written as a product of rate of change in wave vector and partial differential of probability function with respect to the wave vector:

$$\left(\frac{\partial f}{\partial t}\right)_{\text{fields}} = -\left(\frac{\partial \mathbf{k}}{\partial t}\right) \left(\frac{\partial f}{\partial \mathbf{k}}\right). \quad (3.3)$$

This yields the net equation as equation 3.4 and 3.5 which are the Boltzmann Transport Equation (BTE) for energy carriers:

$$\left(\frac{\partial f}{\partial t}\right) = -\mathbf{v} \cdot (\nabla_r f) - \left(\frac{\partial \mathbf{k}}{\partial t}\right) \left(\frac{\partial f}{\partial \mathbf{k}}\right) + \left(\frac{\partial f}{\partial t}\right)_{\text{collisions}} \quad (3.4)$$

or

$$\left(\frac{\partial f}{\partial t}\right) + \mathbf{v} \cdot (\nabla_r f) + \left(\frac{\partial \mathbf{k}}{\partial t}\right) \left(\frac{\partial f}{\partial \mathbf{k}}\right) = \left(\frac{\partial f}{\partial t}\right)_{\text{collisions}}. \quad (3.5)$$

Now, applying the Boltzmann transport equation to phonons, we can ignore the contribution from external fields to the change in probability distribution function. The rate contribution from collisions is solely attributed to the scatterings happening within (note that there are multiple types of scattering processes). If we consider n as the space dependent phonon distribution, then the overall equation now becomes:

$$\left(\frac{\partial n}{\partial t}\right) + \mathbf{v}_g \cdot (\nabla_r n) = \left(\frac{\partial n}{\partial t}\right)_{\text{collisions}}, \quad (3.6)$$

where v_g is the group velocity of phonon wave modes of interest. At steady state, the linearized form of this equation in terms of phonon population deviation is as given in 3.7. This equation formulates a collision matrix to define the rate of change in phonon population distribution under collisions:

$$\mathbf{v}_g \cdot (\nabla_r n) = -\sum_{\nu} \Omega_{\nu} (n_{\nu} - n_{\nu}^0), \quad (3.7)$$

where ν indicates phonon wave vector for each branch, Ω is the collision matrix, and n_0 is the Bose-Einstein distribution at given temperature. If it is assumed that the temperature deviation from the ambient is low, the equilibrium population terms can be expressed using Taylor series expansion while neglecting higher order term as:

$$n_0(T) = n_0(T_0) + \frac{C}{\hbar\omega}(T - T_0), \quad (3.8)$$

where $C = k_B\eta^2(\sinh \eta)^{-2}$ is the mode resolved heat capacity and T_0 is the ambient temperature. Here, the term η is expressed as $\hbar\omega/2k_BT_0$. Phonon temperature deviation is expressed in similar terms as $\Delta T = (\hbar\omega/C)\Delta n$, which simplifies the above equation 3.7 as:

$$C\mathbf{v}_g \cdot (\nabla_r \Delta T) = - \sum_{\nu} W_{\nu}(\Delta T_{\nu}), \quad (3.9)$$

where W_{ν} is the collision scattering operator in terms of energy for a given phonon wave vector, ν . This equation 3.9 is the linearized steady state phonon BTE formulated in terms of temperature deviation from ambient.

3.2.2 Relaxation Time Approximation (RTA)

While the left hand side of the equation 3.9 depends on the phonon dispersion wave modes, the right hand side which includes the scattering operator is complex to quantify. Same is the case with the equation 3.6 where the scattering term on the right hand side of the equation is complex to define. This is due to the multiple wave mode possibilities for phonons in addition to the scattering phenomenon in the thermal transport. Thus, an assumption is chosen to simplify the model depending on the applicability to the material. One such widely used assumption is the Relaxation Time Approximation where the rate of change of phonon population due to internal scattering is calculated as the ratio of population deviation from equilibrium distribution to the relaxation time, τ :

$$\left(\frac{\partial n}{\partial t} \right)_{\text{collisions}} = - \frac{(n - n_0)}{\tau}. \quad (3.10)$$

This approximation, when applied to the phonon temperature deviation, similarly approximates the collision operator formulation to a rate of change of temperature deviation with respect to relaxation time, thus simplifying the linearized steady state phonon BTE expressed in temperature (Equation 3.9) to:

$$\mathbf{v}_g \cdot (\nabla_r \Delta T) = -\frac{\Delta T - \Delta T_l}{\tau}, \quad (3.11)$$

where ΔT_l is the pseudo lattice temperature deviation which is calculated based on energy conservation within the system. This is the governing equation used by the current solver.

3.3 Software Solution Methodology

OpenBTE solves a linear system of equations iteratively to arrive at the required thermal solution for phonon transport in materials. The primary governing equation used here is the relaxation time approximated linearized BTE expressed in terms of phonon temperature deviation (expressed in the equation 3.11). The simulation domain along with the applied boundary conditions are discussed in this section.

3.3.1 Simulation Domain and Boundary Conditions

The simulation starts with a cuboidal lattice domain of chosen dimensions, say l_x , l_y and l_z in the three dimensions, respectively, as shown in Figure 3.1. Periodic boundary conditions are applied at all the major faces. In addition to this, energy conservation is applied at every interface, pore boundary and in the overall lattice. While the energy conservation at the interfaces and pore boundaries helps to solve the thermal properties of incoming and outgoing phonons at those positions, energy conservation on the overall lattice helps to determine the pseudo lattice temperature deviation, ΔT_l . In addition, a temperature gradient in the direction of choice, say X direction, is introduced to initiate heat transfer in the domain.

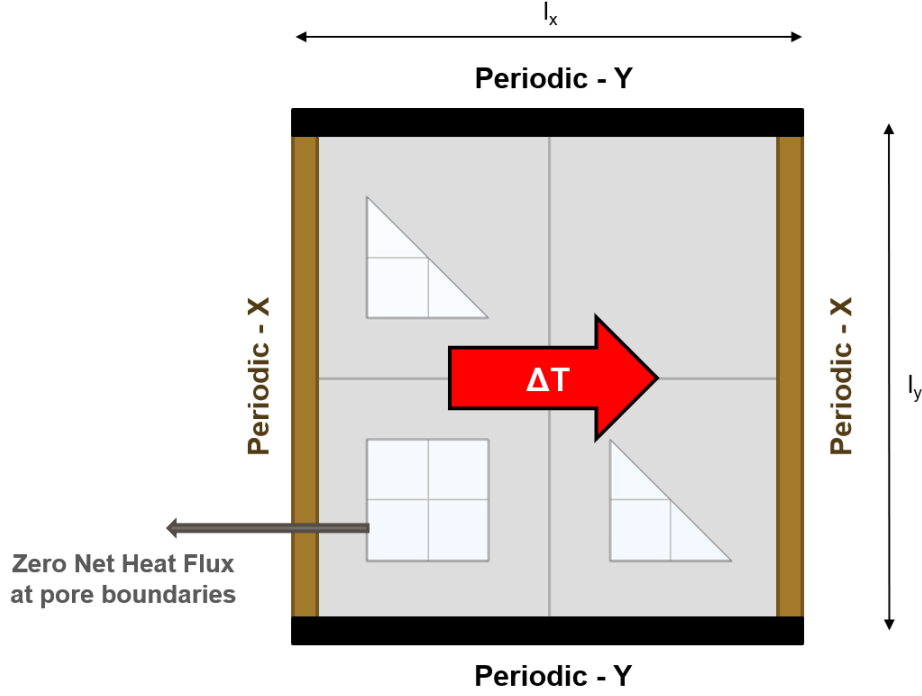


Figure 3.1. A sample simulation domain used in OpenBTE along with the applied boundary conditions.

3.3.2 Solution Framework

Now, with the simulation domain and the boundary conditions in place, the governing equations need to be solved to obtain the thermal properties of the PnC domain of interest. The solution starts with discretizing the linearized BTE under RTA, as in equation 3.11. The equation is discretized using an upwind finite-volume scheme and the phonon modes are resolved. It is then simplified until a system of linear equations are obtained to solve iteratively. All the incoming and outgoing phonons are assumed to thermalize to the same temperature. This is done to further simplify flux calculations in the energy balances. The fourier law of heat conduction is then used to provide the code with an initial estimate of temperature. This discretization of the heat conduction done for both orthogonal as well as complex domains is used to obtain a bulk thermal conductivity estimate. Lastly, the software iteratively solves the system of linear equations using the provided initial guess until it reaches the temperature solution. This temperature data along with the calculated heat

fluxes are utilized to solve for the thermal conductivity contributions from the heat fluxes and the ballistic phonon transport. Finally, the mode resolved as well as the cumulative thermal conductivity values are calculated and reported.

3.3.3 Modules in the Software

While the implementation of the BTE within the software is accurate, a much more impressive feature is its set of modules - Geometry and Material. The entire framework for the software is as shown in the figure 3.2, which is reproduced from [43]. Each of the modules and their submodules are discussed below.

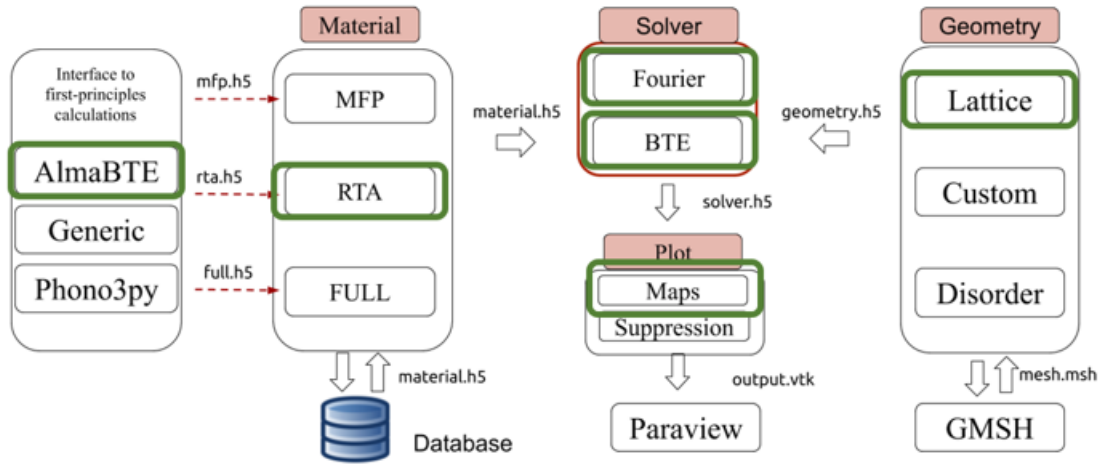


Figure 3.2. Software framework for OpenBTE solver (reproduced from [43]).

Geometry Module

The geometry module is the first package utilized within the solver. It is used to define the simulation domain or the lattice design. Since the solver is designed to be used for wide range of geometry selections, there are different submodules introduced as geometry types within the software. Some of them currently in usage include

- Bulk geometries

- Thin films with custom designed slots
- Complex lattice geometries

Material Module

Once the lattice geometry is defined, the material properties have to be input to the software. This is dealt by the Material module of the package where the mode-resolved bulk phonon dispersion data along with their group velocities, heat capacity and scattering rates for the chosen material are extracted from AlmaBTE or Phono3Py sources which use first principle calculations. These properties are then utilized within the lattice or superlattice builder to obtain properties for the PnC.

RTA-BTE Solver Module

Finally, utilizing the material properties together with the geometry defined, the software iteratively solves the discretized BTE under periodic boundary conditions and an applied temperature gradient in the direction of choice. During this process, Fourier’s law of heat conduction is also solved on the defined geometry to obtain the Fourier thermal conductivity. The temperature and flux values thus calculated can be plotted and the dominant heat flow paths within a custom lattice design can be identified.

3.4 Implementation of Strain in the model and Closure

Since the software utilizes the dispersion plots calculated for pre-strained bulk materials, the strain cannot be modeled directly in this case. The only way to have the software calculate the post-strain thermal conductivity is by inputting a new dispersion plot information for each given lattice under required strain calculated from the first principles. This would also require accurately obtaining the heat capacity and scattering rates. As this is extremely time-consuming, this solver is not used to calculate the post-strain thermal anisotropy, but is only used to evaluate and identify key (heat flux dominant) features in a specific lattice

geometry pre-strain. These results and inferences derived from them are reported in Chapter 6.

4. VARIANCE REDUCED MONTE CARLO METHOD FOR BTE

4.1 Introduction

Monte Carlo methods are statistical methods which are widely used to numerically solve equations. Compared to extensive analytical methods or first principle calculations, they are easier to apply when there are many independent variables in the system. Thus, many researchers have tried to utilize Monte Carlo methods to solve Boltzmann Transport Equation as well. Mazumdar et al. [82] worked on one of the earliest algorithms involving Monte Carlo methods to solve the BTE. While the early works just focused on modeling advection based flow and simple scattering processes [44], [45], more improvements have been made to the scattering operators to increase the accuracy of the model using efficient energy-based formulations. One of the methods with such improvements is the variance reduced Monte Carlo method proposed by Pearaud et al. [83] and later improved based on linearized BTE formulations [84], [85] and ab-initio calculations [86].

Because particle dynamics like phonon transport and scattering can be modeled much easily with Monte Carlo based methods, they offer an advantage compared to other solution techniques. In addition, the effect of scale of the lattice on the computational speed is linear. Any lattice geometry constituting simple features can be modeled in this technique. But this method needs dispersion plots, group velocities, and relaxation times as inputs usually, if not also mean free paths. If these input values are not calculated accurately, the error can carry over to the MC simulation as well. Another disadvantage with the MC method is the computational expense. An appropriate time step has to be chosen and the simulation needs to be run for multiple number of time steps until convergence is achieved. Though the method has its drawbacks and complexities, it has highly capable of modeling particle-like known inter-phonon scattering effects within the lattice, as well as interactions with boundaries.

4.2 MC Methods to Solve BTE - Approach

One of the earliest proposed algorithms to solve BTE using MC methods was by Mazumdar et al. [82]. The approach involved random selection of bundle of phonons simulated across the chosen PnC lattice. The wavemodes and positions are randomly chosen too, and during a time step, they are allowed to undergo ballistic transport first before the scattering was calculated. Different boundary conditions like adiabatic and diffusive surfaces were chosen based on the type of simulation. A small enough time step was selected too to allow phonons to interact within the lattice before they can go out of bounds. The Boltzmann Transport Equation is widely regarded as the fundamental equation governing the transport of phonons. As such, MC methods use the BTE as starting point too. Traditional MC methods use the Relaxation time approximated BTE (combining equations (3.6) and (3.10), as derived in Chapter 3):

$$\left(\frac{\partial n}{\partial t}\right) + \mathbf{v}_g \cdot (\nabla_r n) = -\frac{(n - n_0)}{\tau}.$$

A typical MC algorithm is shown in the Figure 4.1. It is a straightforward step-by-step implementation of phonon progression in time involving the following steps:

1. Simulation domain definition
2. Phonon bundle initialization
3. Phonon mobilization through advection
4. Temperature sampling
5. Phonon scattering

4.2.1 Simulation Domain Definition

The domain chosen as the simulation box is a thin layer of size 10 nm x 10nm and with thickness of one atomic layer (0.335 nm). Periodic heat flux conditions are applied as boundary conditions in the directions other than the heat flow direction such that the

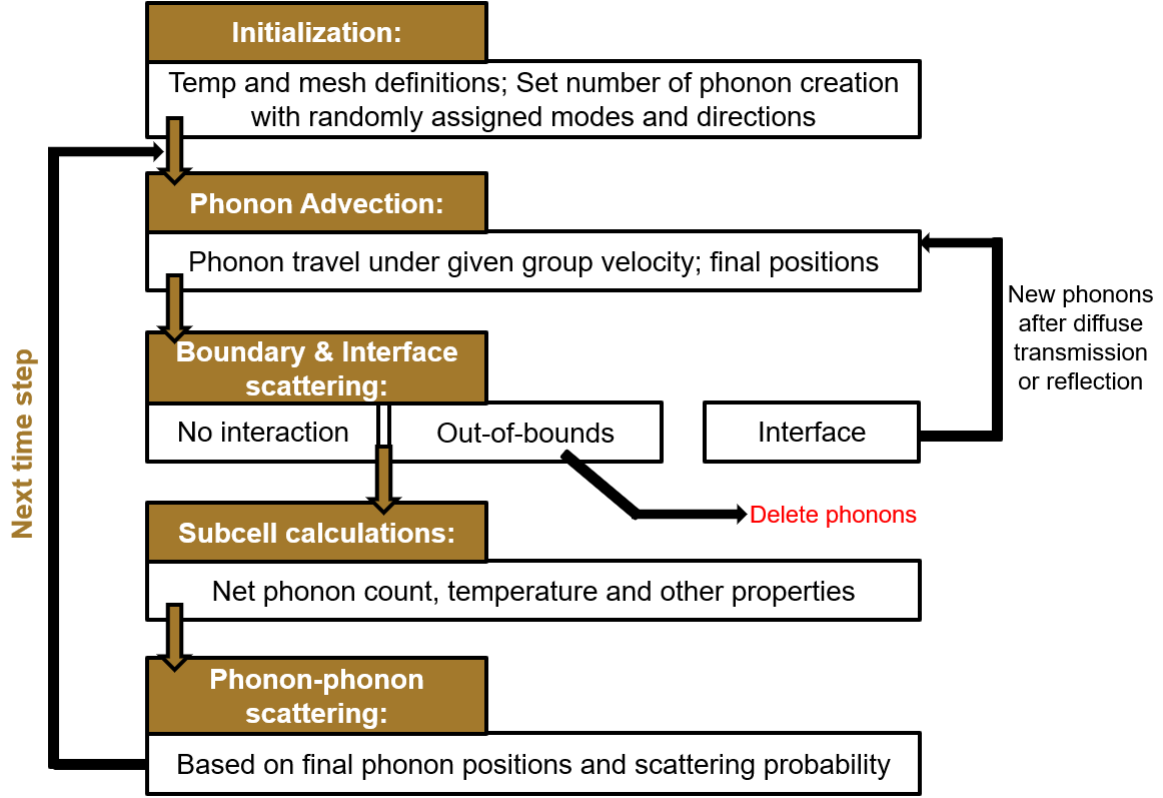


Figure 4.1. A typical algorithm followed by an MC-based BTE solver.

phonons leaving from one side of the lattice can enter from the other side thereby maintaining the periodicity while conserving the energy and momentum balance. On the other hand, a temperature gradient is applied to the faces in the heat flow direction to initialize the heat flow. The major governing equation used here is the BTE expressed in terms of either the phonon population distribution (equation (4.1)) or the phonon energy distribution (equation (4.2)) or the phonon energy deviation (equation (4.3)) as follows:

$$\left(\frac{\partial n}{\partial t}\right) + \mathbf{v}_g \cdot (\nabla_r n) = -\frac{(n - n_0)}{\tau}, \quad (4.1)$$

$$\left(\frac{\partial e}{\partial t}\right) + \mathbf{v}_g \cdot (\nabla_r e) = -\frac{(e - e_0)}{\tau}, \quad (4.2)$$

$$\left(\frac{\partial e_d}{\partial t}\right) + \mathbf{v}_g \cdot (\nabla_r e_d) = -\frac{(e_d - e_{d0})}{\tau}, \quad (4.3)$$

where e , e_0 , e_d , and e_{d0} are phonon energy distribution, equilibrium phonon energy distribution, phonon energy deviation, and equilibrium phonon energy deviation, respectively.

4.2.2 Phonon Bundle Generation

With the thermal boundary conditions in place, a sample simulation domain with dimensions l_x , l_y and l_z look like the domain in the Figure 4.2 below.

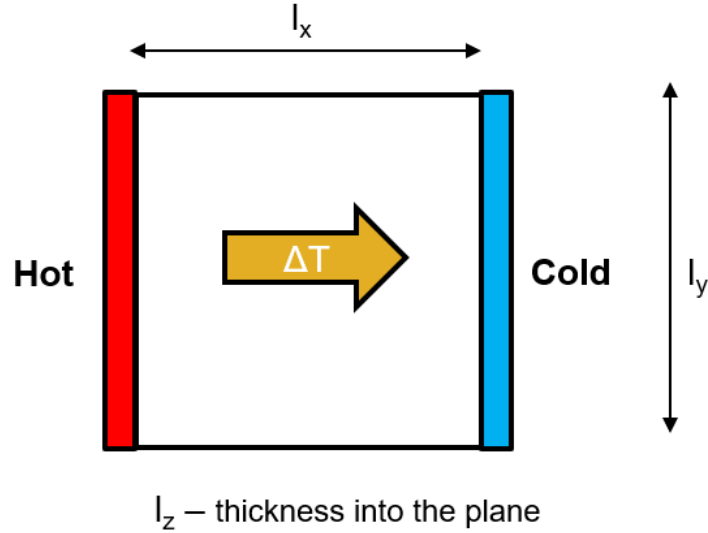


Figure 4.2. A sample lattice domain showing boundary conditions.

Phonons are generated in bundles based on the equilibrium phonon population distribution and their density of states. The Bose-Einstein distribution is usually the distribution function followed while drawing and assigning frequencies to phonons. But, some other methods using energy-based formulations [83] utilize other distributions too, like f_{new} for example:

$$f_{new} = \frac{\hbar\omega \sum_p D}{\exp\left(\frac{\hbar\omega}{k_B T}\right) - 1}. \quad (4.4)$$

Here D , and p are phonon density of states and phonon polarization respectively. Since the optical wave modes do not contribute much to the overall thermal conductivity, only the acoustic wave modes are usually considered as the available phonon states - *i.e* one longitudinal acoustic (LA) mode and two transverse acoustic (TA) modes. A random set of numbers is chosen again to assign random positions and frequencies to each phonon bundle depending on their corresponding distributions and assigned wave modes. From these parameters, quantities like group velocity, density of states, specific heat and relaxation time are calculated as needed. This sets everything up for the advection calculation.

4.2.3 Phonon Mobilization through Advection

With each phonon bundle in place and with their own unique frequency and direction, the first step that happens after the time of the simulation starts is the phonon movement under advection based on their group velocities. This is a very simple process and can be numerically expressed as:

$$\mathbf{u}(t + \Delta t) = \mathbf{u}(t) + \mathbf{v}_g \Delta t. \quad (4.5)$$

Here, Δt , \mathbf{u} and \mathbf{v}_g are simulation time step, position vector and phonon group velocity respectively. During this step, the scattering processes are not yet considered. This step decides the final position of the phonon bundles along with their defined momentum and energy. If phonon advection is interfered either by a boundary (hot or cold wall) or by a geometric feature (pore geometry), phonons undergo reflection or diffuse transmission randomly. If phonons encounters an interface (composite material layer), a similar probability is followed to address their response. This is how boundary and interface scattering is accounted for in the MC methods. After this, the phonon bundles continue moving until the end of the time step and reach their new positions.

4.2.4 Temperature Sampling

With phonon bundles occupying their new positions, the new temperature and pseudo temperature are calculated from the corresponding local energy, E , (equation (4.6)) and pseudo energy, \tilde{E} , (equation (4.7)) expressions as follows respectively:

$$E = V \int_0^{\omega_{max}} \sum_p \frac{D\hbar\omega}{\exp\left(\frac{\hbar\omega}{k_B T}\right) - 1} d\omega, \quad (4.6)$$

$$\tilde{E} = V \int_0^{\omega_{max}} \sum_p \frac{1}{\tau} \frac{D\hbar\omega}{\exp\left(\frac{\hbar\omega}{k_B T}\right) - 1} d\omega, \quad (4.7)$$

where V , D , and p are simulation domain volume, phonon density of states and phonon polarization respectively.

4.2.5 Phonon Internal Scattering

Finally, the simulation at this time step reaches the substep where internal scattering is taken into consideration. While boundary and interface scattering have been accounted for earlier during the advection step based on the phonon position, internal scattering is accounted for based on a probability function called scattering probability, P , for each phonon bundle which is calculated as:

$$P = 1 - \exp\left(-\frac{\Delta t}{\tau}\right). \quad (4.8)$$

Depending on the scattering probability, a set of phonons are chosen to undergo scattering. Since it is a process in which the energy is conserved, different techniques are employed to make sure the conservation is followed. In phonon population based approach, the post-scattering phonon frequencies are randomly chosen. In such cases, the phonon number is increased or reduced to ensure the energy conservation is held. On the other hand, in phonon energy or energy deviation based approaches, the energy is always conserved by treating the number of phonons as a variable. Both the approaches boil down to similar numerical basis after which the simulation carries on to the next time step.

After each time step, the temperature plot is calculated and compared with the plot obtained in the previous time step. The process carries on until the temperature plot does not change with time indicating steady state. Then, the overall simulation box dimensions and the temperature within the box are used together to calculate heat flux or thermal conductivity using an expression similar to the Fourier's law of heat conduction.

4.3 Calculation of Phonon Dispersion Relations

Phonon dispersion relations are very essential to any meta material property calculations where in depth understanding of effect of phonon vibrations is needed. A phonon dispersion relation is a set of functions which describe the relation between phonon frequency (or energy) of different wave modes and the wave vector. Depending on whether the material is isotropic or anisotropic, multiple wave mode curves are obtained. These curves are then used to calculate phonon properties like group velocity, specific heat and relaxation times which in turn aid in estimating the thermal conductivity. Many methods are used to estimate these relations starting from lattice dynamics calculations [61], [62] to scattering experiments [87]. While these experimental and in-depth numerical techniques are very accurate, they are also time consuming or computationally expensive. Thus, in this study, a continuum mechanics based dispersion plot estimation is used to obtain the respective phonon dispersion relation for meta materials with different pore geometries. For the single layer graphene with no pores, the experimental dispersion data is used. The results from the continuum model are validated against this data. The elastic model is then used to estimate dispersion relations for PnCs with different pore geometries. Though this level of estimation for thin films using an elastic model is not very accurate due to phonon confinement, the method is used as an initial evaluator to compare with other more accurate thermal conductivity estimations.

4.3.1 Continuum Mechanics based Phonon Dispersion Relations

In this approach, a geometry domain with the size of the required PnC and with intended pore geometry is built. Assuming that the material is uniform and isotropic, the material properties at given temperature are used as input to the system. Single layer graphene

is anisotropic, but at low strains, the single layer graphene PnC can be modeled as an isotropic material. The equivalent elastic mechanical properties are obtained from molecular mechanics calculations from literature for the current phonon dispersion calculations. The properties used and the references from which they are extracted are shown in the Table 4.1.

Table 4.1. Calculated properties of single layer graphene using molecular mechanics calculations

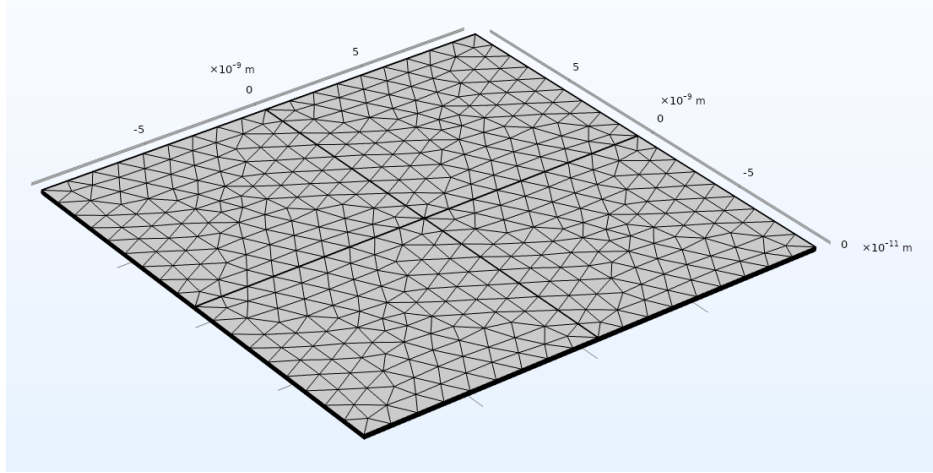
Property Name	Value	Reference
Bond Length	1.42 Å	[73]
Young's Modulus	1022.01 GPa (Zigzag)	[88]
	1023.95 GPa (Armchair)	[88]
Density	2270 kg/m ³	[89]
Poisson's ratio	0.190	[90]

Once the domain is chosen and properties are applied, a swept mesh containing at least 5 layers in thickness direction and required number of elements in the in-plane direction is built. An example lattice geometry with mesh is shown in the Figure 4.3a. As boundary conditions, Floquet-Bloch periodic conditions are used at the in-plane lattice boundaries - with parallel faces being the source and destination respectively. The displacement field at the boundary conditions are as follows:

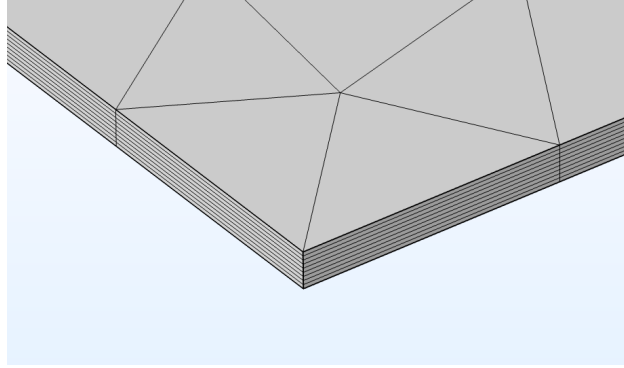
$$\mathbf{u}_{dst} = \mathbf{u}_{src} \exp(-jk_F(\mathbf{r}_{dst} - \mathbf{r}_{src})), \quad (4.9)$$

where \mathbf{u} , j , k_F and \mathbf{r} denote displacement field, square root of negative unity, Floquet wave number and spacial coordinates respectively. Also src and dst represent source and destination respectively. For the boundaries in the thickness direction, traction-free condition is applied. All of these boundary conditions on a sample thin layer lattice is shown in the Figure 4.4.

Now, a parameter k , for wave vector, is defined and this is parametrically swept across the lattice to calculate for their corresponding eigenvalue solutions. The resulting plot of the eigen values with respect to the wave number correspond to the dispersion relationships. To



(a) Domain showing mesh elements.



(b) Domain showing mesh along thickness.

Figure 4.3. A sample lattice with mesh of appropriate element size.

obtain a complete dispersion plot, these resulting eigenvalues have to be plotted for the first Brillouin zone, which is defined by the shaded area in the Figure 4.5.

4.4 Implementation of Strain in the Model

While the heat transfer due to phonons is estimated, the effect of the strain has to be accounted for too. This is where the dispersion plots are utilized. To account for strain, the geometry is left the same as the strain applied is very low. The continuum models are used to calculate the post-strain dispersion relationships for each different pore geometry. These post-strain dispersion relations are substituted as input instead of the original no strained dispersion. The resulting thermal conductivity estimated with these new set of frequencies,

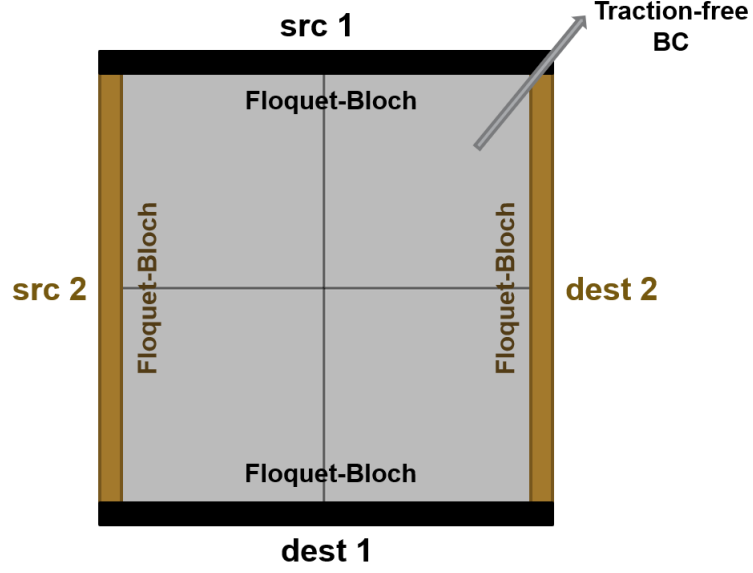


Figure 4.4. A sample domain showing boundary conditions applied.

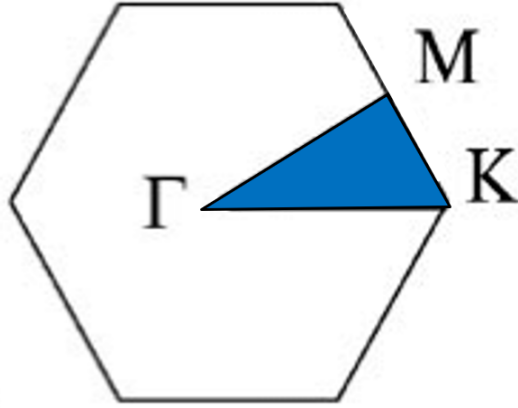


Figure 4.5. Figure showing Brillouin Zone (shaded area) in reciprocal space.

group velocities and density of states is presented as post-strain thermal conductivity prediction from this method. This way of modeling strain in this MC method (shown in Figure 4.6) can be made more accurate if dispersion relations used as input here are calculated from first principles instead of continuum mechanics.

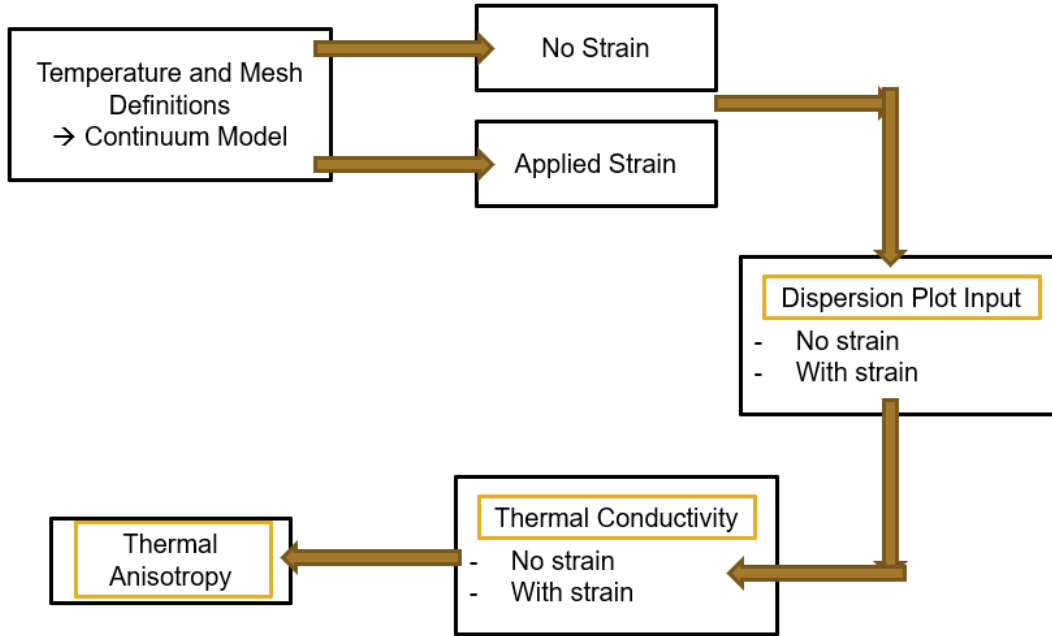


Figure 4.6. Algorithm implemented to obtain pre and post strain dispersion relations.

4.5 Closure

The predicted thermal conductivity values for single layer graphene PnCs with different pore geometries and the validation against experimental data is presented in chapter 6. Along with this, the comparison of this method with other techniques is also presented before addressing the individual effect of group velocities on the thermal conductivity. The next chapter discusses Callaway-Holland model which is another model solving the RTA based steady state Boltzmann Transport Equation.

5. CALLAWAY-HOLLAND MODEL

5.1 Introduction

Thermal transport by phonons is usually understood to be similar to a broadband energy transmission where phonons with multiple wavemodes collectively carry heat across the lattice. Thus understanding phonons, their wave modes and the corresponding dispersion behavior becomes key to cracking the code for estimating the thermal conductivity accurately. An important feature for phonon flow is the mean free path (Λ). The relative comparison between the characteristic length and mean free path given by Knudsen number, Kn , is used to categorize the phonon flow and the corresponding heat transport features.

Modeling phonon flow is a popular topic in heat transfer research. Many researchers have tried to model phonon flow using just dispersion relations attributing to their ballistic transport. Monte Carlo methods were then used to estimate effective heat flux and thermal conductivity [83]. But on an analytical front, most of the research in phonon flow has converged towards applying Boltzmann Transport Equation which is based on conservation of number of particles [29], [42], [43]. In this chapter, one such analytical model is discussed. The phonon dispersion relations are estimated using continuum mechanics – based model. They are then combined with the estimates of the phonon mean free path and scattering times to estimate the effective in-plane thermal conductivity using Callaway-Holland solution to the Boltzmann Transport Equation.

5.2 Governing Transport Equation - BTE

This solver utilizes relaxation time approximated steady state BTE as the governing equation. The simplified general form of BTE as derived in Chapter 3 (see equation 3.6) is as follows:

$$\left(\frac{\partial n}{\partial t}\right) + \mathbf{v}_g \cdot (\nabla_r n) = \left(\frac{\partial n}{\partial t}\right)_{\text{collisions}}, \quad (5.1)$$

where v_g is the phonon group velocity of each mode obtained from dispersion relations. To simplify the collision term on the right hand side of the equation 5.1, the RTA assumption is used which expresses the change in phonon population, n , as an exponential reduction in

deviation from an equilibrium distribution, n_0 . Using this assumption, the collision term on the right hand side can be simplified to the ratio of difference in population distribution to the relaxation time as:

$$(n - n_0) \propto \exp\left(-\frac{t}{\tau}\right)$$

or

$$\left(\frac{\partial n}{\partial t}\right) = -\frac{(n - n_0)}{\tau}, \quad (5.2)$$

where τ is the relaxation time due to the combined effect of all the scattering processes and n_0 is the equilibrium phonon population, at a temperature T , given by Bose-Einstein distribution as:

$$n_0 = \frac{1}{\exp\left(\frac{\hbar\omega}{k_B T}\right) - 1}, \quad (5.3)$$

where \hbar , ω , and k_B are reduced Planck's constant, angular frequency (in rad/s), and Boltzmann constant respectively. Also note that the values of these constants are $\hbar = 1.0546 \times 10^{-34} \text{ Js}$ and $k_B = 1.3806 \times 10^{-23} \text{ J/K}$. This when substituted in the right hand side of the equation 5.1 gives the simplified Boltzmann Transport Equation under Relaxation Time Approximation:

$$\left(\frac{\partial n}{\partial t}\right) + \mathbf{v}_g \cdot (\nabla_r n) = -\frac{(n - n_0)}{\tau}. \quad (5.4)$$

Now, at steady state, the net rate of change of phonon population with time goes to zero. Thus, the above equation 5.4 is further simplified as:

$$\mathbf{v}_g \cdot (\nabla_r n) = -\frac{(n - n_0)}{\tau}. \quad (5.5)$$

This is the steady state Boltzmann transport equation under relaxation time approximation, the fundamental governing equation that is used in Callaway-Holland method to estimate heat flux and thermal conductivity due to the flow of heat carriers (phonons).

5.3 Callaway-Holland Analytical model

The steady state BTE equation obtained earlier has been solved by using multiple techniques including analytical solutions and numerical methods of various accuracy levels. One of such widely used analytical models is Callaway-Holland model. It is an approximate solution where relaxation time, τ , due to scattering is estimated for momentum conserving processes (normal processes) and momentum non-conserving processes (Umklapp scattering, impurity scattering and boundary scattering):

$$\frac{1}{\tau} = \frac{1}{\tau_C} + \frac{1}{\tau_{NC}}, \quad (5.6)$$

where τ_C is relaxation time due to normal processes which conserve momentum, and τ_{NC} is the relaxation due to scattering processes which do not conserve momentum. Note that τ_C is sufficiently large that its overall contribution towards the rate of change of phonon population can be neglected. For the non-conserving processes, Matthiessen's rule is used to estimate the scattering rate due to the combined effect of Umklapp, impurity and boundary scattering as follows:

$$\frac{1}{\tau_{NC}} = \frac{1}{\tau_{Um}} + \frac{1}{\tau_{Im}} + \frac{1}{\tau_{Bo}}, \quad (5.7)$$

where τ_{Um} , τ_{Im} , and τ_{Bo} are relaxation times under Umklapp scattering, impurity scattering, and boundary scattering, respectively. Under the bulk material assumption and in the chosen direction within the metamaterial, the above relaxation time terms are further expressed as:

$$\frac{1}{\tau_{Um}} = C_1 T \omega^2 \exp\left(-\frac{C_2}{T}\right),$$

$$\frac{1}{\tau_{Im}} = C_3 T \omega^4,$$

$$\frac{1}{\tau_{Bo}} = \frac{v}{C_4}, \quad (5.8)$$

where the constants C_1 , C_2 , C_3 , and C_4 are obtained by fitting the thermal conductivity data to the available experimental data. These relaxation time terms depend on the frequency of the phonon wave mode and temperature of the material (*i.e* dispersion relation data). This total scattering rate combined with the summation of energies from all modes using specific heat for each mode gives the overall thermal conductivity solution from Callaway-Holland model:

$$k = \frac{1}{6\pi^2} \sum_i \int_q (C)(v)^2(\tau)q^2 dq, \quad (5.9)$$

where k , i and q are thermal conductivity, wave mode branch index, and phonon wave number, respectively. Here the specific heat value corresponding to each specific phonon branch is again expressed as:

$$C = \frac{\hbar^2 \omega^2}{k_B T^2} \frac{\exp\left(\frac{\hbar \omega}{k_B T}\right)}{\left(\exp\left(\frac{\hbar \omega}{k_B T}\right) - 1\right)^2}. \quad (5.10)$$

Equations 5.9 and 5.10 give the solution for total thermal conductivity estimate from the Callaway-Holland model for Boltzmann transport equation under relaxation time approximation:

$$k = \frac{1}{6\pi^2} \sum_i \int_q \left(\frac{\hbar^2 \omega^2}{k_B T^2} \frac{\exp\left(\frac{\hbar \omega}{k_B T}\right)}{\left(\exp\left(\frac{\hbar \omega}{k_B T}\right) - 1\right)^2} \right) (v)^2(\tau)q^2 dq. \quad (5.11)$$

Every term here is a function of phonon wave vector, frequency, and corresponding group velocities for all phonon branches of interest. This data can be obtained from phonon dispersion relations for the specific metamaterial geometry similarly to the technique discussed in the section 4.3.

5.4 Implementation of Strain in the Model

The continuum model results in an approximate dispersion plot from which the wave modes of interest are extracted and are validated against a set of accurate dispersion plots obtained either from experiments or first principle calculations. The lattice domain is then

strained and the Floquet-Bloch boundary conditions are reapplied to obtain a new set of eigen values for the same wave vector parameters thus giving us the dispersion plots post applied strain. These pre and post strain dispersion relations for the wavemodes of interest are used in the equation 5.5 to predict the effective pre and post-strain thermal conductivity values.

5.5 Closure

The thermal conductivity values predicted using this model are reported in chapter 6. In addition to the comparison with other methods, a detailed investigation of effect of temperature and strain on thermal transport in PnCs is performed and reported too.

6. RESULTS

This chapter compares the different models applied to a single layer graphene (SLG) lattice, and evaluates the impact of different transport and scattering mechanisms.

6.1 Thermal Conductivity Estimation of Single Layer Graphene Lattice

This section compares predictions from different techniques used to model phonon transport at nanoscale. The first part presents the calculated thermal conductivities before strain is applied, while the next part reports the changes to thermal behavior with strain. These are used to then evaluate the sensitivity of phonon transport in single-layer graphene lattices to strain. Though the BTE is a common governing equation for many of the solvers evaluated here, the assumptions and conditions chosen to solve them along with the accuracy of the input data provided in each of the methods affect the overall thermal conductivity estimate compared to the MD simulations that rely only on the input of the interatomic potentials.

6.1.1 Prediction and Validation of Thermal Conductivity from First Principle Calculations

An open source phonon transport solver, called AlmaBTE [42], is used to calculate dispersion data along with the thermal conductivity tensor for a bulk material using first principle calculations. In this work, AlmaBTE solver is used to obtain a set of benchmark thermal conductivity values which will be used later to compare with the thermal conductivity estimations from other techniques. The inputs to this solver include structural parameters of the lattice along with the potential energy values and force constants obtained using first principle calculations. These are directly extracted from the AlmaBTE [42] repository for the current work. Using these quantities, the estimated thermal conductivity for a single layer graphene lattice is shown in the Figure 6.1. It can be seen from the Figure 6.1 that the thermal conductivity estimations here match well with the data from the literature [91], [92], especially above 300K. Based on this validation, the current work will use this thermal conductivity prediction as the validation for the other thermal models.

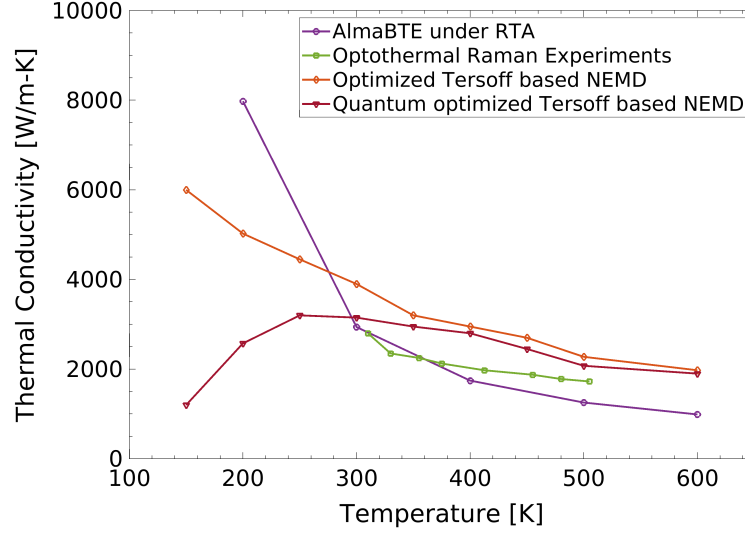


Figure 6.1. Validation of thermal conductivity of SLG calculated from AlmaBTE solver against Opto-thermal experimental data [91] and Tersoff-based NEMD solver output [92].

6.1.2 Thermal Conductivity from Callaway-Holland Method

The Callaway-Holland model predicts the thermal conductivity of the single layer graphene PnC with a given pore geometry using the following equation (recall equation 5.11):

$$k = \frac{1}{6\pi^2} \sum_i \int_q \left(\frac{\hbar^2 \omega^2}{k_B T^2} \frac{\exp\left(\frac{\hbar \omega}{k_B T}\right)}{\left(\exp\left(\frac{\hbar \omega}{k_B T}\right) - 1\right)^2} \right) (v)^2 (\tau) q^2 dq, \quad (6.1)$$

where

$$\tau = \left(C_1 T \omega^2 \exp\left(-\frac{C_2}{T}\right) + C_3 T \omega^4 + \frac{v}{C_4} \right)^{-1}. \quad (6.2)$$

This model needs material dispersion relations as input which is obtained in this work from periodic elastic models in COMSOL. Curve fitting of the bulk single layer graphene thermal conductivity is then used to calculate the constants (C_1 , C_2 , C_3 , and C_4) in the relaxation time terms, where C_4 is the minimum length feature in the lattice. Utilizing the thermal conductivity values from Opto-thermal experimental data [91] to fit the model, the constants are obtained as in Table 6.1.

Table 6.1. Curve-fitted constants for the Callaway-Holland model for Single layer graphene with no pores

Curve fitting parameter	Value
C_1	$3.7 \times 10^{-20} \text{ s/K}$
C_2	303 K
C_3	$1.32 \times 10^{-46} \text{ s}^{-3}$
C_4	$\infty \text{ m}$

The thermal conductivity using these constants are compared against the conductivity values reported from the AlmaBTE solver in the Figure 6.2. Thus the model is calibrated, and is later used to obtain thermal conductivity predictions for SLG PnCs with different pore geometries.

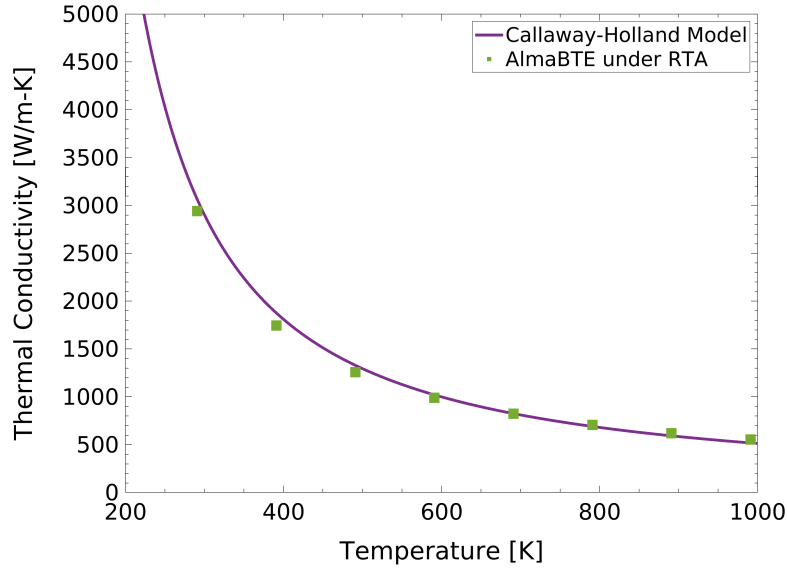


Figure 6.2. Calibration of thermal conductivity of SLG calculated using Callaway-Holland model against AlmaBTE values.

6.1.3 Thermal Conductivity from the Monte Carlo Method

For the variance reduced Monte Carlo (VRMC) method, the thermal conductivity is estimated at each time step until the process reaches steady state. A sample plot for the conductivity calculated at each time step of the simulation is shown in the Figure 6.3. The calculation for a single layer graphene lattice uses a time step of 1 ps and the simulation was run until the steady state in temperature or convergence in the thermal conductivity is reached (approximately for 700 ps here for convergence in thermal conductivity). The conductivity values are compared with the baseline AlmaBTE data in Figure 6.4. It can be seen that the conductivity predictions from MC for SLG lattice with no pores are slightly lower than the AlmaBTE values, but are within the range of reported conductivity values in the literature [91].

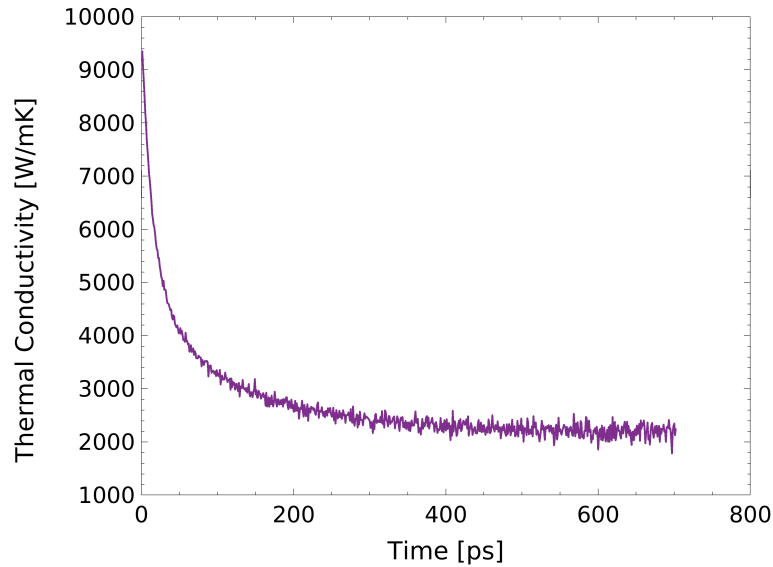


Figure 6.3. Thermal conductivity predictions at each time step in the VRMC simulation.

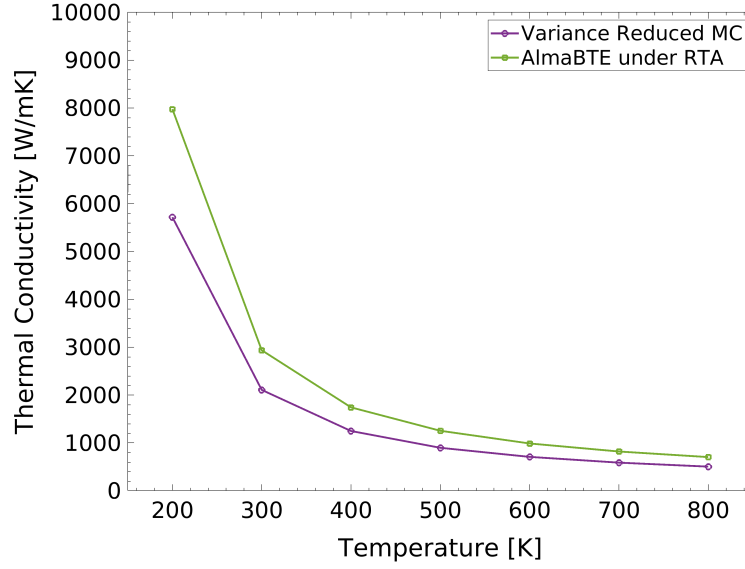


Figure 6.4. Comparison of thermal conductivity of SLG obtained using VRMC model against baseline data from AlmaBTE.

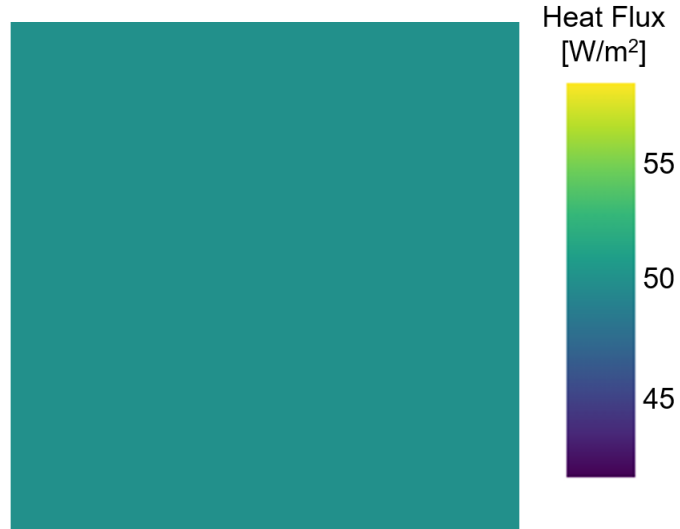


Figure 6.5. Heat Flux of SLG lattice predicted from OpenBTE solver.

6.1.4 Thermal conductivity from OpenBTE solver

Unlike the previous two solvers where an equivalent pore geometry is modeled, the OpenBTE software needs a very specific geometry design as the simulation domain. Since

the lattice is just a single layer graphene PnC, a simple cuboidal domain was defined. The required lattice parameters as well as the potential energy constants are taken from the AlmaBTE source [42]. A temperature gradient of 1 K was applied on the system in the X direction. Using these, the net heat flux output obtained for a simple lattice at a given temperature of 300 K is as shown in the Figure 6.5. The estimated thermal conductivity is at 300K is 2934 W/m-K which matches well with our baseline data and other data from literature.

6.1.5 Thermal Conductivity from Non-Equilibrium Molecular Dynamics

For the NEMD approach, the atom positions in the lattice are defined by using the data from Figure 2.2. The algorithm as detailed in the Figure 2.1 is used. The resultant energy transferred at every time step is shown in the Figure 6.6. As seen in Figure 6.6, the energy

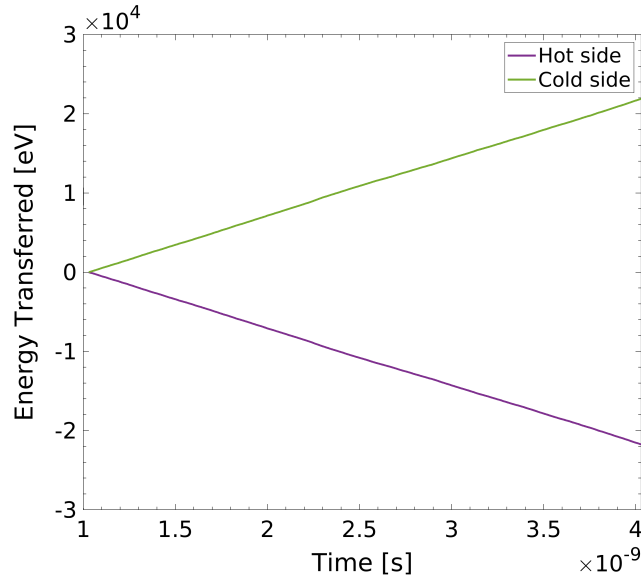


Figure 6.6. Energy in eV transferred at hot and cold regions during each time step of the NEMD simulation.

transferred to both the hot and cold sides is equal and opposite as expected. The slope,

dE_{eV}/dt of these curves gives the net heat transferred which is later used to calculate the heat flux using equation 6.3:

$$q''_{net} = (1.602 \times 10^{-19}) \frac{dE_{eV}/dt}{A_{cross-section}}, \quad (6.3)$$

where $A_{cross-section}$ is the area of cross section of the single layer graphene lattice calculated as the product of inter-layer distance (0.335 nm) and width of the lattice (20 nm). The obtained temperature distribution along the direction of the applied temperature gradient is also shown in the Figure 6.7. To avoid the surface effects, only the interior points are chosen to compute the temperature gradient, dT/dx .

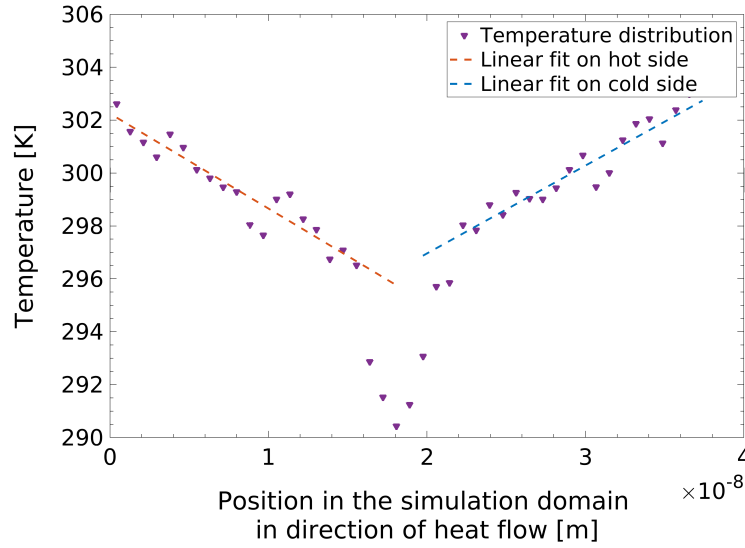


Figure 6.7. Temperature distribution as a function of position within the simulation domain in the direction of heat flow.

The calculated heat flux and temperature gradient values from Figure 6.6 and Figure 6.7 are used to calculate the thermal conductivity of single layer graphene in that particular heat flow direction using equation 6.4:

$$k_{NEMD} = \frac{q''_{net}}{dT/dx}. \quad (6.4)$$

The final reported thermal conductivity from this method at 300K is 1736 W/mK. which is within the range of thermal conductivity reported [91], [93], [94].

6.1.6 Comparison of Predicted Thermal Conductivity

Figure 6.8 compares the predictions from all the methods used in this work. In addition to the predictions from the different solvers, the grey bars represent the experimental limits for SLG thermal conductivity predictions from Xu *et al.* [93] and Li *et al.* [91]. The black bars, on the other hand, represent theoretical conductivity predictions using 3-phonon scattering alone, and 3 and 4 phonon scattering combined from Feng *et al.* [94]. As seen, all the predictions from this work fall between these limits, thus showing the validity of all these models in predicting thermal conductivity for SLG without any pore structure.

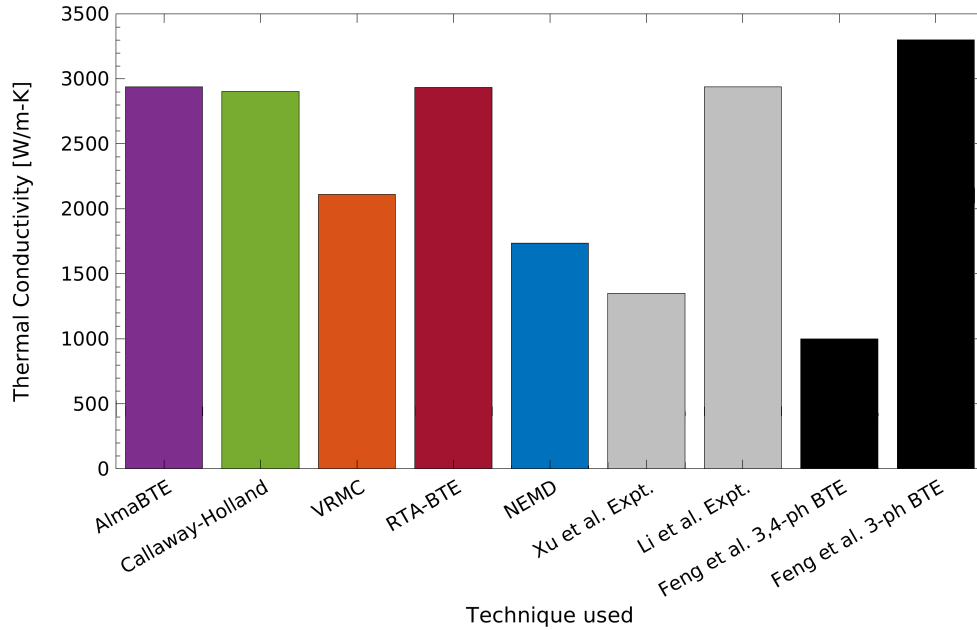


Figure 6.8. Comparison of thermal conductivity predictions at 300 K for SLG sheet with no pores calculated with the experimental [91], [93] and theoretical [94] predictions.

While Figure 6.8 reveals that all the methods reasonably predict the thermal conductivity values of SLG with no pores at 300K. The challenge lies with modeling size effects and interface effects due to various pore geometries which are absent in these initial data. This

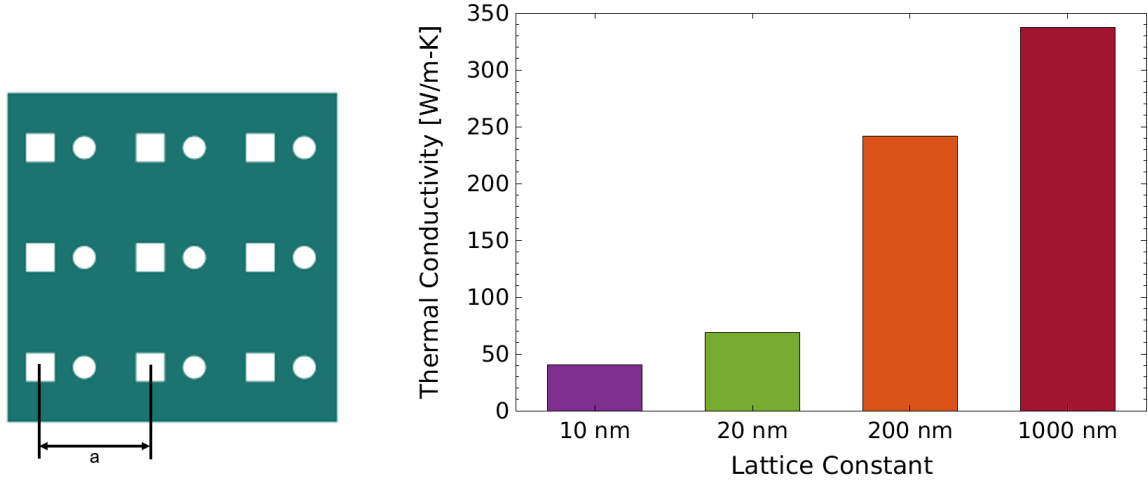
effect of pore geometry is addressed in the later sections. Now, another important parameter to consider while comparing different methods is the total computation time. This, for each method is shown in Table 6.2. As expected, NEMD takes significantly more amount of time for a calculation compared to all other techniques while Callaway-Holland provides the quickest predictions. However, the Callaway-Holland model required calibration against the first-principles calculations (or from experiments) for parameters of the scattering time.

Table 6.2. Computation time for a thermal conductivity prediction for each method

Technique	Computation Time (Approx.)
NEMD	35-40 hrs
RTA based BTE	20-30 mins
Monte Carlo	8-10 hrs
Callaway-Holland	<1 min

6.2 Size Effects on the Thermal Conductivity of Single Layer Graphene

While the thermal conductivity estimates for an SLG with no pores are consistent with literature, additional complexity in solving phonon transport comes from including the pore boundaries and interfaces within the system. Any pore feature added to the lattice affects the Mean Free Path (MFP) of phonons thereby affecting the thermal conductivity. Though this effect is negligible at macroscale, it becomes increasingly significant as the simulation domain is scaled down to a nanometer level. For a sample lattice with an arbitrary pore design (see Figure 6.9a(a)), the thermal conductivity estimated using the RTA-BTE method reduces as the size of the repeating element reduces (see Figure 6.9b). This can be explained based on the cumulative thermal conductivity distribution. As illustrated by data from AlmaBTE (as shown in the Figure 6.10), phonons with very small MFPs (in nanometer range) contribute minimally to the overall thermal conductivity compared to the longer MFP phonons. As the lattice size approaches the phonon MFP, collisions are significantly impacted, thereby drastically reducing the phonons carrying heat across the lattice.



(a) Lattice with defined random pore geometry. (b) Size effects seen in thermal conductivity predictions (from RTA-BTE method).

Figure 6.9. A lattice with random pore geometry and the corresponding size effects on thermal conductivity.

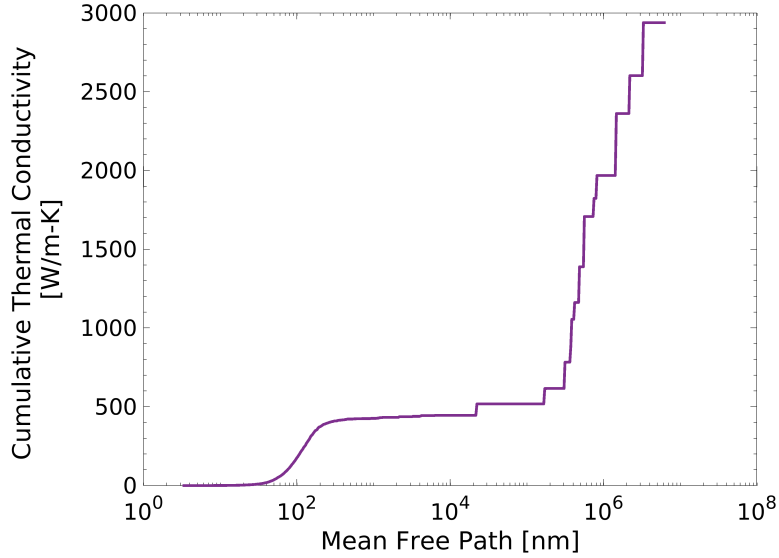


Figure 6.10. Cumulative thermal conductivity of SLG as a function of phonon MFP from AlmaBTE.

6.3 Thermal Conductivity for Lattices with Different Pore Geometries

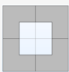
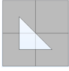




Because the phonon transport is a mixture of diffuse phonon flow as well as the ballistic transport, boundary scattering including the impact of pore shape play a key role in thermal

transport. In addition to this, the size effects detailed in the previous subsection presses more the need for an accurate phonon transport model especially at nanoscale. In order to further understand the accuracy of the techniques discussed in the previous chapters, this work compares the thermal conductivity estimations from each of those techniques for SLG lattices with selected pore geometries.

6.3.1 Thermal Conductivity Prediction Results

Table 6.3 shows the lattice designs and their thermal conductivity predicted from different techniques. The first three techniques assume that the single layer graphene is isotropic in the plane. So, the overall conductivity prediction only has one reported value. For the last technique, NEMD, the heat flow direction is chosen to be in the armchair direction and thus reports the conductivity value in that direction for comparison with results from other techniques.

Table 6.3. Estimated Thermal Conductivity values for Single Layer Graphene lattices (20nm x 20nm) with different pore geometries

Thermal Conductivity Predictions [W/mK]				
Lattice	Callaway-Holland	VRMC	RTA-BTE	NEMD
1 	26	490	35	126
2 	27	497	46	116
3 	14	484	32	118
4 	13	475	24	77
5 	11	458	20	75
6 	8	442	20	81

The data from the NEMD method is chosen as the standard to compare the results from other techniques. Based on the different assumptions and characteristics of each model, we find the following key conclusions:

- **Failure of Callaway-Holland Model to Predict the Size Effects Accurately:**

As seen from the data, the thermal conductivity predictions from the Callaway-Holland model fail to accurately account for size effects of the lattice and thus overpredict the reduction in conductivity. This is due to the model being simplified to function for bulk materials and thin layers with the specific pore geometry being included as a characteristic length term in the phonon-boundary scattering rate calculation.

- **Inaccurate Prediction of the Size Effect with the Current Version of the VRMC Method:**

The VRMC method, on the other hand, considers the overall size effects. But as this model only includes an equivalent geometry based on the average boundary-boundary distance to define the pore boundary scattering, some of the boundary scattering effects are not accounted for thereby leading to inaccurate thermal conductivity predictions. This can be fixed by updating the model by including an accurate pore boundary model within the code while also having accurate scattering rate definitions.

- **Overprediction of Size Effects in RTA-BTE Solver:**

Finally the RTA-based BTE solver accounts for the size effects as well as the pore boundary effects, but overpredicts their effect on the thermal conductivity, thus reducing the predicted values. This indicates that the linearized BTE formulation with considered assumptions may not be the best combination to model the thermal transport in graphene.

These inferences help understand that while NEMD is the more accurate, it is also computationally expensive. And the Callaway-Holland model used here with individual dispersion plots can only be accurate up to a certain level unless geometry is accounted for more into the scattering rate. Monte Carlo methods with geometry included as well as an accurate RTA-BTE solver can account for scattering effects as long as care is taken to input

correct material dispersion data. While advanced MC methods need to have more definitions of scattering to account for all possible processes within the lattice, RTA-BTE solvers need to omit certain assumptions taken to improve the thermal conductivity predictions.

6.4 Modeling the Effect of Strain on SLG PnC Thermal Conductivity

In this section, the effect of strain on thermal conductivity of single layer graphene lattices is estimated using the four different techniques. The phonon transport is modeled for the simple lattice designs. By utilizing the results for each of the lattices, the study aims to understand the possible features affecting the phonon transport under strain.

6.4.1 Methodology

Here, all of the techniques previously discussed are brought together to understand the effect of strain on a SLG lattice in detail while also identifying guidelines to design a lattice with pore geometry which is the most thermally sensitive under applied strain. A uniaxial strain of 6 % is applied in the X-direction on the lattice to determine the effect on the thermal conductivity change in X and Y directions. Depending on the technique used, the effects taken into consideration are different and therefore are separately evaluated. This separation of effects and the overall combination is shown through a chart in the Figure [6.11](#) (refer to Figure [1.1](#) in Chapter 1).

6.4.2 Impact of Strain on Thermal Conductivity

Phonon transport predictions are computed on each lattice before and after strain. The effect of strain on a given PnC is reported in terms of their pre and post-strain thermal conductivity values. These are predicted from each method separately and are presented in the Tables [6.4](#) and [6.5](#). In NEMD method, the X direction is the zigzag direction while the Y direction is the armchair direction. In MC and Callaway-Holland models, on the other hand, the single layer graphene is treated as isotropic initially and the approximate in-plane conductivity values are predicted accordingly.

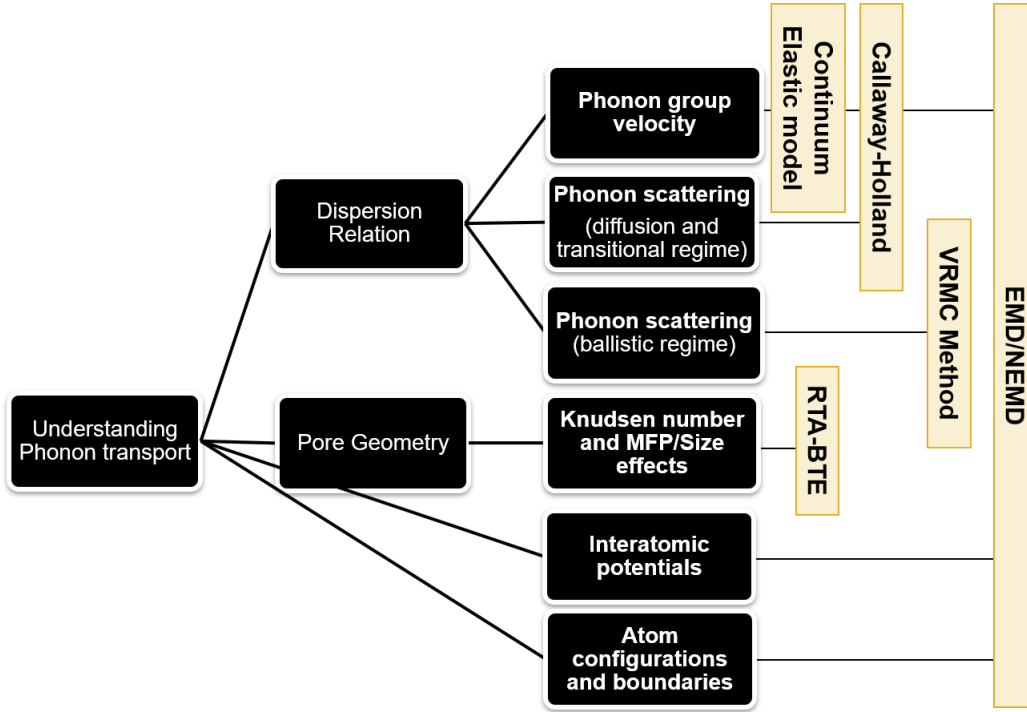


Figure 6.11. Illustration of methods to predict thermal transport and which strain-dependent transport mechanisms are included.

Table 6.4. Thermal conductivity under uniaxial strain of 6% for Single Layer Graphene lattices (20nm x 20nm) with different pore geometries (predicted using NEMD).

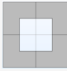





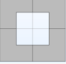





Pre-strain		Post-strain	
Lattice	$k_{X\text{-pre}}$ (zigzag)	$k_{Y\text{-pre}}$ (armchair)	$k_{X\text{-post}}$ (zigzag)
1 	161	126	148
2 	156	116	133
3 	252	118	211
4 	97	77	82
5 	93	75	84
6 	100	81	91

Table 6.5. Thermal conductivity under uniaxial strain of 6% for Single Layer Graphene lattices (20nm x 20nm) with different pore geometries (predicted using Monte Carlo and Callaway-Holland models).

Lattice	Monte-Carlo			Callaway-Holland		
	k_{pre}	k_{X-post}	k_{Y-post}	k_{pre}	k_{X-post}	k_{Y-post}
1 	490	471	478	26	26	27
2 	497	479	484	27	27	27
3 	484	466	473	14	14	14
4 	475	459	469	13	13	13
5 	458	442	457	11	11	11
6 	442	427	441	8	8	8

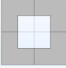





As seen from the conductivity values presented, the reported magnitudes and deviations vary significantly between different methods. NEMD includes the most physics and should be the most complete representation of the strain effect. Every other technique represents predictions with some error. As such, there needs to be a common parameter which can be compared between different methods to gauge the effect of strain as a whole. This leads to in-plane thermal conductivity anisotropy (defined as $A = k_Y/k_X$) for each of the PnCs.

6.4.3 Impact of Strain on Thermal Transport Anisotropy

The overall strain effect on each lattice is reported in terms of change in the in-plane thermal anisotropy, which is defined as $(A_{post} - A_{pre})/A_{pre} * 100$, where A is the in-plane thermal anisotropy, *pre* and *post* represent the pre-strain and post-strain conductivity predictions. The deviation in the anisotropy for an SLG lattice with no pore geometry is about 5.8% (using NEMD) which can be attributed solely to the effect of strain on the group velocities, lattice geometry and molecular structure. Now, the anisotropy deviations for PnCs

with chosen pore geometries from NEMD are expressed as deviations from this zero deviation. The, thus calculated anisotropy deviations along with the same predictions from other methods are reported in the Table 6.6. For methods other than NEMD, the models initially consider the PnC to be isotropic and hence the post-strain thermal anisotropy is directly reported as the final in-plane thermal anisotropy deviation due to strain.

Table 6.6. Estimated Thermal Anisotropy Deviations under uniaxial strain of 6% for Single Layer Graphene lattices (20nm x 20nm) with different pore geometries

Thermal Anisotropy Deviation % [-]				
Lattice	Velocity change	Callaway-Holland	VRMC	NEMD
1 	6.4 %	2.3 %	1.5 %	1.2 %
2 	4.9 %	2.9 %	1.1 %	7.1 %
3 	5.2 %	2.5 %	1.7 %	3.1 %
4 	5.0 %	1.3 %	2.2 %	8.2 %
5 	6.6 %	1.6 %	3.5 %	2.7 %
6 	6.2 %	1.2 %	3.2 %	2.5 %

As seen from the Table 6.6, the reported deviations also vary significantly between methods. NEMD is the most accurate representation of the strain effect and is used to compare the other methods' reported anisotropy deviations to evaluate the effectiveness of each of those methods. In addition to this, to understand the impact of strain, first, the heat flux plots for each chosen lattice design using the RTA-BTE solver are reported and the dominant heat flow paths are identified as shown in the Figure 6.12. These heat flow paths hold the key to understanding the strain effect on the SLG lattice.

Based on the results from the table 6.6 along with the heat flux distributions from 6.12, the following inferences can be made about the internal scattering effects:

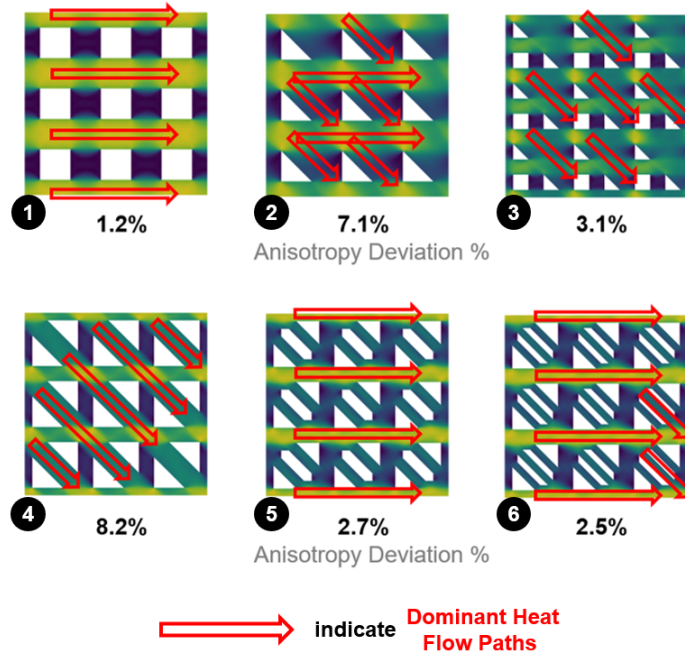


Figure 6.12. Dominant heat flow paths (indicated by red arrows) based on heat flux distributions in each lattice calculated from the OpenBTE solver.

- **Effect of the Assumption of Isotropic Band Structures and the Effect of Material Properties:**

As seen from the data, the predicted deviations in thermal anisotropy predicted by the Callaway-Holland and VRMC models are smaller than the deviations predicted by the NEMD model. This may be due to the isotropic assumption considered to obtain the effective material modulus and Poisson's ratio, which yielded inaccurate dispersion relations. Since the major input to both the models here is the dispersion relation, any inaccuracy in them may lead to errors in the eventual thermal conductivity and anisotropy prediction.

- **Effect of Dominant Heat Flow Paths:**

The heat flux results from OpenBTE represent a much more accurate way of explaining the effect of pore geometry on the thermal conductivity. Though the effect of strain cannot be modeled well using this solver for now, the dominant heat flow paths identified from it lay the foundation to understanding the phonon transport within the

SLG lattice at the nanometer scale. From Figure 6.12, it can be seen that when the majority of dominant heat flow paths are aligned with the applied strain direction, the overall anisotropy deviation under applied strain is low compared to the cases where dominant heat flow paths are aligned at an angle to the applied strain leading to more thermal anisotropy deviation.

- **Effect of pore geometry in ballistic transport view point:**

In addition to the dominant heat flow paths, the geometry itself affects the phonon flow. This is because, at nanoscale with multiple nanopores in the lattice, phonon transport tends to be in the ballistic regime. The material bridges caused by nanopores and the change in their geometry under this applied strain affect the thermal conductivity and heat flow.

6.4.4 Combined Effects of Lattice Size, Pore Geometry, and Heat Flow Paths

Finally, the predicted deviations in thermal anisotropy from the NEMD simulations provide more insight.

- For the lattices with non-aligned pore geometry and containing more dominant heat flow paths aligned at an angle to the applied strain, the effects due to each complement and stack up thus causing the highest thermal sensitivity under applied strain. This is particularly evident in lattice design 2 and 4.
- The opposite effect can be seen with the lattice design 1, where the geometry is completely symmetric and the heat flow paths are perfectly aligned with the strain direction. In this lattice, the group velocity changes and the corresponding pore boundary scattering do not become very significant. This leads to less deviation in the thermal anisotropy.
- While the non-aligned geometry holds the key to higher strain sensitivity, in some cases it can oppose the impact of strain. This can be seen in cases like lattice design 5 and 6 where too much scattering in the thermal bridges lessens the impact of strain on the overall thermal transport.

6.5 Closure

This chapter reports in detail the thermal conductivity predictions from each method before and after the application of strain. The lattice predictions before strain are used to gain an understanding of the applicability of different techniques. Then, the strained conductivity studies are used to explore the factors affecting the thermal conductivity of SLG layers with different pore geometries and under applied strain. This enabled identification of features that promote large changes to the thermal anisotropy.

7. CONCLUSION

7.1 Conclusion

This work investigates the applicability of different phonon transport models to single-layer graphene with and without strain. While the conductivity predictions without strain for a virgin single layer graphene layer using the different methods compare well with experimental data, the difference between the techniques is clearly observed when different pore geometries are introduced. For a lattice without any pores, all the techniques predict a thermal conductivity of about $2900 \text{ W}/(\text{m K})$ at a temperature of 300 K . The conductivity beyond that temperature decreases as the temperature increases, which is typical for such materials. While NEMD predicts the lowest conductivity, it is still within the range of reported conductivities for single layer graphene lattice.

For lattices with pores on the other hand, these solvers predict vastly different conductivity values. With conductivity predictions from NEMD considered as the most accurate prediction, all other predictions are compared against the NEMD data. Firstly, for Callaway-Holland model, it can be clearly seen that the model involves simplifications applicable to a bulk material or a thin layer material with no complex pore geometry. The domain is also considered continuous with no option to include geometry. This lack of consideration for size and boundary scattering effects is also reflected in the conductivity predictions from the model as they are very low compared to the NEMD values. The variance reduced Monte Carlo method on the other hand considers a simplified pore geometry within the module and does not model all the pore boundaries. This means that much of the internal scattering is omitted. This is observed with the conductivity predictions from the method too as they are larger than the NEMD predictions. Though the current conductivity predictions are not very accurate, Monte Carlo methods are the most reliable solvers to model phonon transport due to the ease of including any and all known additional phonon interaction phenomena. They also have reduced simulation time for larger simulation domains.

The RTA-based BTE solver, OpenBTE, has one of the most detailed solutions to the Boltzmann Transport Equation. The decision to deterministically solve the BTE involved the solver dealing with multiple complex boundary conditions along with intricate partial

differential equations. Due to this, some assumptions were considered like common phonon thermalizing temperature, and uniform isotropic material. These set of assumptions together affect the thermal predictions by a lot especially when high level of scattering is involved. That, exactly, is observed with the OpenBTE thermal conductivity predictions which are lower than the expected NEMD values. This result indicates that while RTA-BTE solvers account for geometry, size effects, and internal scattering, they need more refinement to accurately predict the phonon transport.

With strained lattices, since the conductivity predictions varied a lot for each technique, a common parameter, in-plane thermal anisotropy deviation, is considered to indicate the effect of strain on the lattice. This term expresses the change in thermal anisotropy of single layer graphene as it is strained. From the anisotropy deviation results obtained from every technique, inferences similar to those of pre-strained predictions can be drawn. The Callaway-Holland model which does not accurately address the size effects fails to address the strain effect accurately. VRMC method manages to predict some of the deviations. This is very similar to the conductivity predictions, as the inclusion of the simplified pore geometry accounts for some of the internal scattering. The RTA-BTE solver on the other hand, though not useful in modeling strain, becomes useful as an initial evaluator tool to identify the effect of strain based on the dominant heat flow paths concept. This along with the ballistic view point on the geometry paves way to understanding the effect of strain on phononic crystals in the order of nanometers. Based on these inferences, both the MC methods and RTA-BTE solvers could become accurate thermal transport predictors replacing computationally expensive MD techniques if they are further developed in the mentioned directions.

7.2 Contribution

This work focuses on specifically understanding the phonon transport at nanoscale while also commenting on the type of solver capable of modeling the factors affecting it. The size effects, or the MFP effects, were reported along with the cumulative thermal conductivity calculations to validate the idea. The work also introduces the concept of dominant heat flow paths in tandem with the pore boundary geometry to explain the nanolevel phonon

flow. In addition, the advantages of using different solvers, and their drawbacks are reported in detail. That section also reports the lacking area in each solver while identifying the effects within those solvers that account for differences in the calculations. This is reported to ensure the future work is steered in the right direction to address the scattering effects. By using lattices with simple pore geometries, the thesis presents multiple factors affecting the thermal conductivity of the phononic crystal. It also presents ways to model the effect of strain on thermal conductivity of a lattice and correspondingly the thermal anisotropy. Finally, the factors to be taken into consideration to design a lattice sensitive to strain are laid out based on the inferences drawn from the results of each technique. With this work, the author hopes to add more perspective to the phonon flow in thin layers, especially single layer graphene, and the effect of strain and other parameters on its thermal behavior.

7.3 Future Work

Since the current work is very investigative and fundamental, the later part of the study can be extended in the following directions:

- **A solver to accurately model the phonon flow:**

As an extension to the first half of the work involving investigating different solvers to model the phonon flow, the next step to be taken can be to work on developing either an MC based model or an RTA-BTE solver. An MC solver which accounts for the pore geometry accurately can resolve the case. A technique to obtain more accurate dispersion plots will also help sharpen the accuracy of such model. On the other hand, the RTA-BTE models need focused work on developing new set of assumptions or scattering operators to account for more effects while not increasing the complexity and cost of the model.

- **Expanding the work to other materials:**

As phonon transport is studied in a material like single layer graphene, a study to expand this knowledge towards other materials and later to composites can be another good direction to move to as enough fundamental knowledge on phonons is lacking in these fields. In addition to this, exploring different types of materials can also bring

out more challenges to be addressed in phonon flow which would help develop a much better phonon transport model later.

- **Lattice design for specific thermoelectric applications and Experiments:**

Based on the knowledge gained so far, the research can also be steered in a direction of designing meta materials to specifically address different thermoelectric applications. This may involve static or dynamic tuning of thermal conductivity and thermal anisotropy in the material. In addition to this, designing experiments to study and validate these designs also contribute to adding more phonon transport knowledge to the community. Silicon is an ideal material to experiment with, but since an NEMD study cannot be conducted on it due to computational limitations, an accurate model can either be built from experimental data or by using the knowledge of phonon flow in other materials.

REFERENCES

- [1] M. Nomura, Y. Kage, D. Müller, D. Moser, and O. Paul, “Electrical and thermal properties of polycrystalline si thin films with phononic crystal nanopatterning for thermoelectric applications,” *Applied Physics Letters*, vol. 106, no. 22, p. 223 106, 2015. DOI: [10.1063/1.4922198](https://doi.org/10.1063/1.4922198). eprint: <https://doi.org/10.1063/1.4922198>. [Online]. Available: <https://doi.org/10.1063/1.4922198>.
- [2] Y. Yin, K. Baskaran, and A. Tiwari, “A review of strategies for developing promising thermoelectric materials by controlling thermal conduction,” *physica status solidi (a)*, vol. 216, no. 14, p. 1 800 904, 2019. DOI: <https://doi.org/10.1002/pssa.201800904>. eprint: <https://onlinelibrary.wiley.com/doi/pdf/10.1002/pssa.201800904>. [Online]. Available: <https://onlinelibrary.wiley.com/doi/abs/10.1002/pssa.201800904>.
- [3] B. F. Donovan, E. Sachet, J.-P. Maria, and P. E. Hopkins, “Interplay between mass-impurity and vacancy phonon scattering effects on the thermal conductivity of doped cadmium oxide,” *Applied Physics Letters*, vol. 108, no. 2, p. 021 901, 2016. DOI: [10.1063/1.4939652](https://doi.org/10.1063/1.4939652). eprint: <https://doi.org/10.1063/1.4939652>. [Online]. Available: <https://doi.org/10.1063/1.4939652>.
- [4] H. M. Masrura, A. Kareekunanan, F. Liu, *et al.*, “Design of graphene phononic crystals for heat phonon engineering,” *Micromachines*, vol. 11, no. 7, 2020, ISSN: 2072-666X. DOI: [10.3390/mi11070655](https://www.mdpi.com/2072-666X/11/7/655). [Online]. Available: <https://www.mdpi.com/2072-666X/11/7/655>.
- [5] Z. Wei, G. Wehmeyer, C. Dames, and Y. Chen, “Geometric tuning of thermal conductivity in three-dimensional anisotropic phononic crystals,” *Nanoscale*, vol. 8, pp. 16 612–16 620, 37 2016. DOI: [10.1039/C6NR04199J](https://doi.org/10.1039/C6NR04199J). [Online]. Available: <http://dx.doi.org/10.1039/C6NR04199J>.
- [6] Y. Li, X. Zhou, Z. Bian, Y. Xing, and J. Song, “Thermal tuning of the interfacial adhesive layer on the band gaps in a one-dimensional phononic crystal,” *Composite Structures*, vol. 172, pp. 311–318, 2017, ISSN: 0263-8223. DOI: <https://doi.org/10.1016/j.compstruct.2017.03.092>. [Online]. Available: <https://www.sciencedirect.com/science/article/pii/S0263822317300284>.
- [7] Q. Liang, Y.-L. He, Q. Ren, Y.-P. Zhou, and T. Xie, “A detailed study on phonon transport in thin silicon membranes with phononic crystal nanostructures,” *Applied Energy*, vol. 227, pp. 731–741, 2018, Transformative Innovations for a Sustainable Future – Part III, ISSN: 0306-2619. DOI: <https://doi.org/10.1016/j.apenergy.2017.07.083>. [Online]. Available: <https://www.sciencedirect.com/science/article/pii/S0306261917309558>.

- [8] R. Anufriev and M. Nomura, “Phonon and heat transport control using pillar-based phononic crystals,” *Science and Technology of Advanced Materials*, vol. 19, no. 1, pp. 863–870, 2018, PMID: 30479674. DOI: [10.1080/14686996.2018.1542524](https://doi.org/10.1080/14686996.2018.1542524). eprint: <https://doi.org/10.1080/14686996.2018.1542524>. [Online]. Available: <https://doi.org/10.1080/14686996.2018.1542524>.
- [9] J. Kirchhof, K. Weinel, S. Heeg, *et al.*, “Tunable graphene phononic crystal,” *Nano Letters*, Feb. 2021. DOI: [10.1021/acs.nanolett.0c04986](https://doi.org/10.1021/acs.nanolett.0c04986).
- [10] M. Sledzinska, B. Graczykowski, J. Maire, E. Chavez-Angel, C. M. Sotomayor-Torres, and F. Alzina, “2d phononic crystals: Progress and prospects in hypersound and thermal transport engineering,” *Advanced Functional Materials*, vol. 30, no. 8, p. 1904434, 2020. DOI: <https://doi.org/10.1002/adfm.201904434>. eprint: <https://onlinelibrary.wiley.com/doi/pdf/10.1002/adfm.201904434>. [Online]. Available: <https://onlinelibrary.wiley.com/doi/abs/10.1002/adfm.201904434>.
- [11] A. Mehaney and A. M. Ahmed, “Theoretical design of porous phononic crystal sensor for detecting co2 pollutions in air,” *Physica E: Low-dimensional Systems and Nanostructures*, vol. 124, p. 114353, 2020, ISSN: 1386-9477. DOI: <https://doi.org/10.1016/j.physe.2020.114353>. [Online]. Available: <https://www.sciencedirect.com/science/article/pii/S1386947720308389>.
- [12] E. M. Dede, P. Schmalenberg, T. Nomura, and M. Ishigaki, “Design of anisotropic thermal conductivity in multilayer printed circuit boards,” *IEEE Transactions on Components, Packaging and Manufacturing Technology*, vol. 5, no. 12, pp. 1763–1774, 2015. DOI: [10.1109/TCPMT.2015.2473103](https://doi.org/10.1109/TCPMT.2015.2473103).
- [13] E. M. Dede, T. Nomura, P. Schmalenberg, and J. Seung Lee, “Heat flux cloaking, focusing, and reversal in ultra-thin composites considering conduction-convection effects,” *Applied Physics Letters*, vol. 103, no. 6, p. 063501, 2013. DOI: [10.1063/1.4816775](https://doi.org/10.1063/1.4816775). eprint: <https://doi.org/10.1063/1.4816775>. [Online]. Available: <https://doi.org/10.1063/1.4816775>.
- [14] E. M. Dede, F. Zhou, P. Schmalenberg, and T. Nomura, “Thermal Metamaterials for Heat Flow Control in Electronics,” *Journal of Electronic Packaging*, vol. 140, no. 1, Mar. 2018, 010904, ISSN: 1043-7398. DOI: [10.1115/1.4039020](https://doi.org/10.1115/1.4039020). eprint: https://asmedigitalcollection.asme.org/electronicpackaging/article-pdf/140/1/010904/6417088/ep_140_01_010904.pdf. [Online]. Available: <https://doi.org/10.1115/1.4039020>.
- [15] I. Quotane, E. H. El Boudouti, and B. Djafari-Rouhani, “Graphene-based one-dimensional terahertz phononic crystal: Band structures and surface modes,” *Nanomaterials*, vol. 10, no. 11, 2020, ISSN: 2079-4991. DOI: [10.3390/nano10112205](https://doi.org/10.3390/nano10112205). [Online]. Available: <https://www.mdpi.com/2079-4991/10/11/2205>.

- [16] D. Feng, W. Jiang, D. Xu, B. Xiong, and Y. Wang, “Micro-silicon phononic crystal with locally resonant theory,” *Applied Physics Letters*, vol. 110, no. 17, p. 171 902, 2017. DOI: [10.1063/1.4981121](https://doi.org/10.1063/1.4981121). eprint: <https://doi.org/10.1063/1.4981121>. [Online]. Available: <https://doi.org/10.1063/1.4981121>.
- [17] F.-H. Bao, L.-L. Bao, X.-Y. Li, *et al.*, “Multi-stage phononic crystal structure for anchor-loss reduction of thin-film piezoelectric-on-silicon microelectromechanical-system resonator,” *Applied Physics Express*, vol. 11, no. 6, p. 067 201, May 2018. DOI: [10.7567/apex.11.067201](https://doi.org/10.7567/apex.11.067201). [Online]. Available: <https://doi.org/10.7567/apex.11.067201>.
- [18] Y. Wang, J. Lee, Y. Xie, X.-Q. Zheng, and P. X.-L. Feng, “High-frequency hexagonal boron nitride (h-bn) phononic waveguides,” in *2019 IEEE 32nd International Conference on Micro Electro Mechanical Systems (MEMS)*, 2019, pp. 319–322. DOI: [10.1109/MEMSYS.2019.8870808](https://doi.org/10.1109/MEMSYS.2019.8870808).
- [19] Y. Wang, J. Lee, X. Zheng, Y. Xie, and P. Feng, “Hexagonal boron nitride phononic crystal waveguides,” *ACS Photonics*, vol. 2019, Oct. 2019. DOI: [10.1021/acsphotonics.9b01094](https://doi.org/10.1021/acsphotonics.9b01094).
- [20] B. Liu, L. Bai, E. Korznikova, S. Dmitriev, A. Law, and K. Zhou, “Thermal conductivity and tensile response of phosphorene nanosheets with vacancy defects,” *The Journal of Physical Chemistry C*, vol. 121, Jun. 2017. DOI: [10.1021/acs.jpcc.7b02933](https://doi.org/10.1021/acs.jpcc.7b02933).
- [21] W. Xu and G. Zhang, “Remarkable reduction of thermal conductivity in phosphorene phononic crystal,” *Journal of physics. Condensed matter : an Institute of Physics journal*, vol. 28, p. 175 401, Apr. 2016. DOI: [10.1088/0953-8984/28/17/175401](https://doi.org/10.1088/0953-8984/28/17/175401).
- [22] W. Xu, L. Zhu, Y. Cai, G. Zhang, and B. Li, “Direction dependent thermal conductivity of monolayer phosphorene: Parameterization of stillinger-weber potential and molecular dynamics study,” *Journal of Applied Physics*, vol. 117, no. 21, p. 214 308, 2015. DOI: [10.1063/1.4922118](https://doi.org/10.1063/1.4922118). eprint: <https://doi.org/10.1063/1.4922118>. [Online]. Available: <https://doi.org/10.1063/1.4922118>.
- [23] H. Meng, D. Ma, X. Yu, L. Zhang, Z. Sun, and N. Yang, “Thermal conductivity of molybdenum disulfide nanotube from molecular dynamics simulations,” *International Journal of Heat and Mass Transfer*, vol. 145, p. 118 719, 2019, ISSN: 0017-9310. DOI: <https://doi.org/10.1016/j.ijheatmasstransfer.2019.118719>. [Online]. Available: <https://www.sciencedirect.com/science/article/pii/S0017931019333630>.
- [24] S. Ge, X. Liu, X. Qiao, *et al.*, “Coherent longitudinal acoustic phonon approaching thz frequency in multilayer molybdenum disulphide,” *Scientific reports*, vol. 4, p. 5722, Jul. 2014. DOI: [10.1038/srep05722](https://doi.org/10.1038/srep05722).

- [25] A. Alexeev, A. Krivosheeva, V. Shaposhnikov, and V. Borisenko, “Calculation of phonon spectra of two-dimensional crystals of molybdenum disulfide and ditelluride,” *Journal of Applied Spectroscopy*, vol. 83, Jan. 2017. DOI: [10.1007/s10812-017-0403-9](https://doi.org/10.1007/s10812-017-0403-9).
- [26] Y. Ouyang, Z. Zhang, D. Li, J. Chen, and G. Zhang, “Emerging theory, materials, and screening methods: New opportunities for promoting thermoelectric performance,” *Annalen der Physik*, vol. 531, no. 4, p. 1 800 437, 2019. DOI: <https://doi.org/10.1002/andp.201800437>. eprint: <https://onlinelibrary.wiley.com/doi/pdf/10.1002/andp.201800437>. [Online]. Available: <https://onlinelibrary.wiley.com/doi/abs/10.1002/andp.201800437>.
- [27] Z. Jin, Q. Liao, H. Fang, *et al.*, “A revisit to high thermoelectric performance of single-layer mos₂,” *Scientific Reports*, vol. 5, Apr. 2015. DOI: [10.1038/srep18342](https://doi.org/10.1038/srep18342).
- [28] J. Callaway, “Model for lattice thermal conductivity at low temperatures,” *Phys. Rev.*, vol. 113, pp. 1046–1051, 4 Feb. 1959. DOI: [10.1103/PhysRev.113.1046](https://doi.org/10.1103/PhysRev.113.1046). [Online]. Available: <https://link.aps.org/doi/10.1103/PhysRev.113.1046>.
- [29] M. G. Holland, “Analysis of lattice thermal conductivity,” *Phys. Rev.*, vol. 132, pp. 2461–2471, 6 Dec. 1963. DOI: [10.1103/PhysRev.132.2461](https://doi.org/10.1103/PhysRev.132.2461). [Online]. Available: <https://link.aps.org/doi/10.1103/PhysRev.132.2461>.
- [30] M. G. Holland, “Phonon scattering in semiconductors from thermal conductivity studies,” *Phys. Rev.*, vol. 134, A471–A480, 2A Apr. 1964. DOI: [10.1103/PhysRev.134.A471](https://doi.org/10.1103/PhysRev.134.A471). [Online]. Available: <https://link.aps.org/doi/10.1103/PhysRev.134.A471>.
- [31] G. Kresse, J. Furthmüller, and J. Hafner, “Ab initio force constant approach to phonon dispersion relations of diamond and graphite,” *EPL (Europhysics Letters)*, vol. 32, p. 729, Jul. 2007. DOI: [10.1209/0295-5075/32/9/005](https://doi.org/10.1209/0295-5075/32/9/005).
- [32] L. T. Kong, “Phonon dispersion measured directly from molecular dynamics simulations,” *Computer Physics Communications*, vol. 182, no. 10, pp. 2201–2207, 2011, ISSN: 0010-4655. DOI: <https://doi.org/10.1016/j.cpc.2011.04.019>. [Online]. Available: <https://www.sciencedirect.com/science/article/pii/S0010465511001500>.
- [33] J. V. Goicochea, M. Madrid, and C. Amon, “Thermal Properties for Bulk Silicon Based on the Determination of Relaxation Times Using Molecular Dynamics,” *Journal of Heat Transfer*, vol. 132, no. 1, Oct. 2009, 012401, ISSN: 0022-1481. DOI: [10.1115/1.3211853](https://doi.org/10.1115/1.3211853). eprint: https://asmedigitalcollection.asme.org/heattransfer/article-pdf/132/1/012401/5648666/012401_1.pdf. [Online]. Available: <https://doi.org/10.1115/1.3211853>.

- [34] J. E. Turney, E. S. Landry, A. J. H. McGaughey, and C. H. Amon, “Predicting phonon properties and thermal conductivity from anharmonic lattice dynamics calculations and molecular dynamics simulations,” *Phys. Rev. B*, vol. 79, p. 064301, 6 Feb. 2009. DOI: [10.1103/PhysRevB.79.064301](https://doi.org/10.1103/PhysRevB.79.064301). [Online]. Available: <https://link.aps.org/doi/10.1103/PhysRevB.79.064301>.
- [35] Y. Ni, Y. Chalopin, and S. Volz, “Calculation of inter-plane thermal resistance of few-layer graphene from equilibrium molecular dynamics simulations,” *Journal of Physics Conference Series*, vol. 395, p. 012106, Nov. 2012. DOI: [10.1088/1742-6596/395/1/012106](https://doi.org/10.1088/1742-6596/395/1/012106).
- [36] K. R. Hahn, C. Melis, and L. Colombo, “Thermal transport in nanocrystalline graphene investigated by approach-to-equilibrium molecular dynamics simulations,” *Carbon*, vol. 96, pp. 429–438, 2016, ISSN: 0008-6223. DOI: <https://doi.org/10.1016/j.carbon.2015.09.070>. [Online]. Available: <https://www.sciencedirect.com/science/article/pii/S0008622315302888>.
- [37] C. Si, X.-D. Wang, Z. Fan, Z.-H. Feng, and B.-Y. Cao, “Impacts of potential models on calculating the thermal conductivity of graphene using non-equilibrium molecular dynamics simulations,” *International Journal of Heat and Mass Transfer*, vol. 107, pp. 450–460, 2017, ISSN: 0017-9310. DOI: <https://doi.org/10.1016/j.ijheatmasstransfer.2016.11.065>. [Online]. Available: <https://www.sciencedirect.com/science/article/pii/S0017931016320154>.
- [38] S. Bazrafshan and A. Rajabpour, “Thermal transport engineering in amorphous graphene: Non-equilibrium molecular dynamics study,” *International Journal of Heat and Mass Transfer*, vol. 112, pp. 379–386, 2017, ISSN: 0017-9310. DOI: <https://doi.org/10.1016/j.ijheatmasstransfer.2017.04.127>. [Online]. Available: <https://www.sciencedirect.com/science/article/pii/S0017931017301783>.
- [39] M. S. El-Genk, K. Talaat, and B. J. Cowen, “Thermal conductivity of silicon using reverse non-equilibrium molecular dynamics,” *Journal of Applied Physics*, vol. 123, no. 20, p. 205104, 2018. DOI: [10.1063/1.5030871](https://doi.org/10.1063/1.5030871). eprint: <https://doi.org/10.1063/1.5030871>. [Online]. Available: <https://doi.org/10.1063/1.5030871>.
- [40] A. S. M. J. Islam, M. S. Islam, N. Ferdous, J. Park, and A. Hashimoto, “Vacancy-induced thermal transport in two-dimensional silicon carbide: A reverse non-equilibrium molecular dynamics study,” *Phys. Chem. Chem. Phys.*, vol. 22, pp. 13592–13602, 24 2020. DOI: [10.1039/D0CP00990C](https://doi.org/10.1039/D0CP00990C). [Online]. Available: <http://dx.doi.org/10.1039/D0CP00990C>.
- [41] W. Li, J. Carrete, N. A. Katcho, and N. Mingo, “Shengbte: A solver of the boltzmann transport equation for phonons,” *Computer Physics Communications*, vol. 185, no. 6, pp. 1747–1758, 2014, ISSN: 0010-4655. DOI: <https://doi.org/10.1016/j.cpc.2014.02.015>. [Online]. Available: <https://www.sciencedirect.com/science/article/pii/S0010465514000484>.

- [42] J. Carrete, B. Vermeersch, A. Katre, *et al.*, “Almabte : A solver of the space–time dependent boltzmann transport equation for phonons in structured materials,” *Computer Physics Communications*, vol. 220, pp. 351–362, 2017, ISSN: 0010-4655. DOI: <https://doi.org/10.1016/j.cpc.2017.06.023>. [Online]. Available: <https://www.sciencedirect.com/science/article/pii/S0010465517302059>.
- [43] G. Romano, “OpenBTE: A Multiscale Solver for the Phonon Boltzmann Transport Equation,” in *APS March Meeting Abstracts*, ser. APS Meeting Abstracts, vol. 2019, Jan. 2019, T70.321, T70.321.
- [44] D. Lacroix, K. Joulain, and D. Lemonnier, “Monte carlo transient phonon transport in silicon and germanium at nanoscales,” *Phys. Rev. B*, vol. 72, p. 064305, 6 Aug. 2005. DOI: [10.1103/PhysRevB.72.064305](https://doi.org/10.1103/PhysRevB.72.064305). [Online]. Available: <https://link.aps.org/doi/10.1103/PhysRevB.72.064305>.
- [45] A. Mittal and S. Mazumder, “Monte Carlo Study of Phonon Heat Conduction in Silicon Thin Films Including Contributions of Optical Phonons,” *Journal of Heat Transfer*, vol. 132, no. 5, Mar. 2010, 052402, ISSN: 0022-1481. DOI: [10.1115/1.4000447](https://doi.org/10.1115/1.4000447). eprint: https://asmedigitalcollection.asme.org/heattransfer/article-pdf/132/5/052402/6608883/052402__1.pdf. [Online]. Available: <https://doi.org/10.1115/1.4000447>.
- [46] A. M. Goto, E. D. Nóbrega, F. N. Pereira, and J. M. C. Dos Santos, “Numerical and experimental investigation of phononic crystals via wave-based higher-order rod models,” *International Journal of Mechanical Sciences*, vol. 181, p. 105776, 2020, ISSN: 0020-7403. DOI: <https://doi.org/10.1016/j.ijmecsci.2020.105776>. [Online]. Available: <https://www.sciencedirect.com/science/article/pii/S002074032030761X>.
- [47] T. Guo, X. Yang, Q. Geng, *et al.*, “Anisotropic phononic crystal structure with low-frequency bandgap and heat flux manipulation,” *Science China Physics, Mechanics & Astronomy*, vol. 63, Feb. 2020. DOI: [10.1007/s11433-019-9437-x](https://doi.org/10.1007/s11433-019-9437-x).
- [48] Z. Chen, X. Zhang, and Y. Pei, “Manipulation of phonon transport in thermoelectrics,” *Advanced Materials*, vol. 30, no. 17, p. 1705617, 2018. DOI: <https://doi.org/10.1002/adma.201705617>. eprint: <https://onlinelibrary.wiley.com/doi/pdf/10.1002/adma.201705617>. [Online]. Available: <https://onlinelibrary.wiley.com/doi/abs/10.1002/adma.201705617>.
- [49] K. Gordiz and A. Henry, “Phonon transport at interfaces between different phases of silicon and germanium,” *Journal of Applied Physics*, vol. 121, no. 2, p. 025102, 2017. DOI: [10.1063/1.4973573](https://doi.org/10.1063/1.4973573). eprint: <https://doi.org/10.1063/1.4973573>. [Online]. Available: <https://doi.org/10.1063/1.4973573>.
- [50] Z. Yan, M. Yoon, and S. Kumar, “Influence of defects and doping on phonon transport properties of monolayer mose2,” *2D Materials*, vol. 5, Apr. 2018. DOI: [10.1088/2053-1583/aabd54](https://doi.org/10.1088/2053-1583/aabd54).

- [51] Z. Zhang, Y. Ouyang, Y. Cheng, J. Chen, N. Li, and G. Zhang, “Size-dependent phononic thermal transport in low-dimensional nanomaterials,” *Physics Reports*, vol. 860, pp. 1–26, 2020, Size-dependent phononic thermal transport in low-dimensional nanomaterials, ISSN: 0370-1573. DOI: <https://doi.org/10.1016/j.physrep.2020.03.001>. [Online]. Available: <https://www.sciencedirect.com/science/article/pii/S0370157320300922>.
- [52] D. Q. Tran, R. Delgado-Carrascon, J. F. Muth, *et al.*, “Phonon-boundary scattering and thermal transport in alxga1–xn: Effect of layer thickness,” *Applied Physics Letters*, vol. 117, no. 25, p. 252 102, 2020. DOI: [10.1063/5.0031404](https://doi.org/10.1063/5.0031404). eprint: <https://doi.org/10.1063/5.0031404>. [Online]. Available: <https://doi.org/10.1063/5.0031404>.
- [53] S. V. J. Narumanchi, J. Y. Murthy, and C. H. Amon, “Comparison of Different Phonon Transport Models for Predicting Heat Conduction in Silicon-on-Insulator Transistors,” *Journal of Heat Transfer*, vol. 127, no. 7, pp. 713–723, Mar. 2005, ISSN: 0022-1481. DOI: [10.1115/1.1924571](https://doi.org/10.1115/1.1924571). eprint: https://asmedigitalcollection.asme.org/heattransfer/article-pdf/127/7/713/5538272/713_1.pdf. [Online]. Available: <https://doi.org/10.1115/1.1924571>.
- [54] Y. Guo and M. Wang, “Lattice boltzmann modeling of phonon transport,” *Journal of Computational Physics*, vol. 315, pp. 1–15, 2016, ISSN: 0021-9991. DOI: <https://doi.org/10.1016/j.jcp.2016.03.041>. [Online]. Available: <https://www.sciencedirect.com/science/article/pii/S0021999116001935>.
- [55] A. McGaughey and M. Kaviani, “Phonon transport in molecular dynamics simulations: Formulation and thermal conductivity prediction,” in ser. *Advances in Heat Transfer*, G. A. Greene, J. P. Hartnett†, A. Bar-Cohen, and Y. I. Cho, Eds., vol. 39, Elsevier, 2006, pp. 169–255. DOI: [https://doi.org/10.1016/S0065-2717\(06\)39002-8](https://doi.org/10.1016/S0065-2717(06)39002-8). [Online]. Available: <https://www.sciencedirect.com/science/article/pii/S0065271706390028>.
- [56] A. Minnich, “Advances in the measurement and computation of thermal phonon transport properties,” *Journal of physics. Condensed matter : an Institute of Physics journal*, vol. 27, p. 053 202, Feb. 2015. DOI: [10.1088/0953-8984/27/5/053202](https://doi.org/10.1088/0953-8984/27/5/053202).
- [57] D. Ma, A. Arora, S. Deng, G. Xie, J. Shiomi, and N. Yang, “Quantifying phonon particle and wave transport in silicon nanophononic metamaterial with cross junction,” *Materials Today Physics*, vol. 8, pp. 56–61, 2019, ISSN: 2542-5293. DOI: <https://doi.org/10.1016/j.mtphys.2019.01.002>. [Online]. Available: <https://www.sciencedirect.com/science/article/pii/S2542529318301615>.
- [58] D. Chakraborty, H. Karamitaheri, L. de Sousa Oliveira, and N. Neophytou, “Effect of wave versus particle phonon nature in thermal transport through nanostructures,” *Computational Materials Science*, vol. 180, p. 109 712, 2020, ISSN: 0927-0256. DOI: <https://doi.org/10.1016/j.commatsci.2020.109712>. [Online]. Available: <https://www.sciencedirect.com/science/article/pii/S0927025620302032>.

- [59] J. Maire, R. Anufriev, R. Yanagisawa, A. Ramiere, S. Volz, and M. Nomura, “Heat conduction tuning by wave nature of phonons,” *Science Advances*, vol. 3, no. 8, e1700027, 2017. DOI: [10.1126/sciadv.1700027](https://doi.org/10.1126/sciadv.1700027). eprint: <https://www.science.org/doi/pdf/10.1126/sciadv.1700027>. [Online]. Available: <https://www.science.org/doi/abs/10.1126/sciadv.1700027>.
- [60] B. Saha, Y. R. Koh, J. P. Feser, *et al.*, “Phonon wave effects in the thermal transport of epitaxial tin/(al,sc)n metal/semiconductor superlattices,” *Journal of Applied Physics*, vol. 121, no. 1, p. 015 109, 2017. DOI: [10.1063/1.4973681](https://doi.org/10.1063/1.4973681). eprint: <https://doi.org/10.1063/1.4973681>. [Online]. Available: <https://doi.org/10.1063/1.4973681>.
- [61] J. A. Thomas, J. E. Turney, R. M. Iutzi, C. H. Amon, and A. J. H. McGaughey, “Predicting phonon dispersion relations and lifetimes from the spectral energy density,” *Phys. Rev. B*, vol. 81, p. 081 411, 8 Feb. 2010. DOI: [10.1103/PhysRevB.81.081411](https://doi.org/10.1103/PhysRevB.81.081411). [Online]. Available: <https://link.aps.org/doi/10.1103/PhysRevB.81.081411>.
- [62] R. Ramírez and C. P. Herrero, “Phonon dispersion in two-dimensional solids from atomic probability distributions,” *The Journal of Chemical Physics*, vol. 151, no. 22, p. 224 107, 2019. DOI: [10.1063/1.5132419](https://doi.org/10.1063/1.5132419). eprint: <https://doi.org/10.1063/1.5132419>. [Online]. Available: <https://doi.org/10.1063/1.5132419>.
- [63] A.-X. Zhang, J.-T. Liu, S.-D. Guo, and H.-C. Li, “Strain effects on phonon transport in antimonene investigated using a first-principles study,” *Phys. Chem. Chem. Phys.*, vol. 19, pp. 14 520–14 526, 22 2017. DOI: [10.1039/C7CP02486J](https://doi.org/10.1039/C7CP02486J). [Online]. Available: <http://dx.doi.org/10.1039/C7CP02486J>.
- [64] Y. Zeng, C.-L. Lo, S. Zhang, Z. Chen, and A. Marconnet, “Dynamically tunable thermal transport in polycrystalline graphene by strain engineering,” *Carbon*, vol. 158, pp. 63–68, 2020, ISSN: 0008-6223. DOI: <https://doi.org/10.1016/j.carbon.2019.11.060>. [Online]. Available: <https://www.sciencedirect.com/science/article/pii/S0008622319311923>.
- [65] R. Gopal, R. Kumar, and A. Parashar, “Tersoff potential with improved accuracy for simulating graphene in molecular dynamics environment,” *Materials Research Express*, vol. 3, p. 035 011, Mar. 2016. DOI: [10.1088/2053-1591/3/3/035011](https://doi.org/10.1088/2053-1591/3/3/035011).
- [66] R. Kumar, R. Gopal, and A. Parashar, “Optimised cut-off function for tersoff-like potentials for a bn nanosheet: A molecular dynamics study,” *Nanotechnology*, vol. 27, p. 085 706, Feb. 2016. DOI: [10.1088/0957-4484/27/8/085706](https://doi.org/10.1088/0957-4484/27/8/085706).
- [67] W. Xu, L. Zhu, Y. Cai, G. Zhang, and B. Li, “Direction dependent thermal conductivity of monolayer phosphorene: Parameterization of stillinger-weber potential and molecular dynamics study,” *Journal of Applied Physics*, vol. 117, no. 21, p. 214 308, 2015. DOI: [10.1063/1.4922118](https://doi.org/10.1063/1.4922118). eprint: <https://doi.org/10.1063/1.4922118>. [Online]. Available: <https://doi.org/10.1063/1.4922118>.

- [68] J.-W. Jiang, H. S. Park, and T. Rabczuk, “Molecular dynamics simulations of single-layer molybdenum disulphide (mos2): Stillinger-weber parametrization, mechanical properties, and thermal conductivity,” *Journal of Applied Physics*, vol. 114, no. 6, p. 064307, 2013. DOI: [10.1063/1.4818414](https://doi.org/10.1063/1.4818414). eprint: <https://doi.org/10.1063/1.4818414>. [Online]. Available: <https://doi.org/10.1063/1.4818414>.
- [69] J.-H. (Zou, Z.-Q. (Ye, and B.-Y. (Cao, “Phonon thermal properties of graphene from molecular dynamics using different potentials,” *The Journal of Chemical Physics*, vol. 145, no. 13, p. 134705, 2016. DOI: [10.1063/1.4963918](https://doi.org/10.1063/1.4963918). eprint: <https://doi.org/10.1063/1.4963918>. [Online]. Available: <https://doi.org/10.1063/1.4963918>.
- [70] K. Govers, S. Lemehov, M. Hou, and M. Verwerft, “Comparison of interatomic potentials for uo2: Part ii: Molecular dynamics simulations,” *Journal of Nuclear Materials*, vol. 376, no. 1, pp. 66–77, 2008, ISSN: 0022-3115. DOI: <https://doi.org/10.1016/j.jnucmat.2008.01.023>. [Online]. Available: <https://www.sciencedirect.com/science/article/pii/S0022311508000986>.
- [71] M. S. Green, “Markoff random processes and the statistical mechanics of time-dependent phenomena. ii. irreversible processes in fluids,” *The Journal of Chemical Physics*, vol. 22, no. 3, pp. 398–413, 1954. DOI: [10.1063/1.1740082](https://doi.org/10.1063/1.1740082). eprint: <https://doi.org/10.1063/1.1740082>. [Online]. Available: <https://doi.org/10.1063/1.1740082>.
- [72] R. Kubo, “Statistical-mechanical theory of irreversible processes. i. general theory and simple applications to magnetic and conduction problems,” *Journal of the Physical Society of Japan*, vol. 12, no. 6, pp. 570–586, 1957. DOI: [10.1143/JPSJ.12.570](https://doi.org/10.1143/JPSJ.12.570). eprint: <https://doi.org/10.1143/JPSJ.12.570>. [Online]. Available: <https://doi.org/10.1143/JPSJ.12.570>.
- [73] S. Hembacher, F. Giessibl, J. Mannhart, and C. Quate, “Revealing the hidden atom in graphite by low-temperature atomic force microscopy,” *Proceedings of the National Academy of Sciences of the United States of America*, vol. 100, pp. 12539–42, Nov. 2003. DOI: [10.1073/pnas.2134173100](https://doi.org/10.1073/pnas.2134173100).
- [74] S. Plimpton, “Fast parallel algorithms for short-range molecular dynamics,” *Journal of Computational Physics*, vol. 117, no. 1, pp. 1–19, 1995, ISSN: 0021-9991. DOI: <https://doi.org/10.1006/jcph.1995.1039>. [Online]. Available: <https://www.sciencedirect.com/science/article/pii/S002199918571039X>.
- [75] D. A. Broido, M. Malorny, G. Birner, N. Mingo, and D. A. Stewart, “Intrinsic lattice thermal conductivity of semiconductors from first principles,” *Applied Physics Letters*, vol. 91, no. 23, p. 231922, 2007. DOI: [10.1063/1.2822891](https://doi.org/10.1063/1.2822891). eprint: <https://doi.org/10.1063/1.2822891>. [Online]. Available: <https://doi.org/10.1063/1.2822891>.

- [76] B. D. Kong, S. Paul, M. B. Nardelli, and K. W. Kim, “First-principles analysis of lattice thermal conductivity in monolayer and bilayer graphene,” *Phys. Rev. B*, vol. 80, p. 033406, 3 Jul. 2009. DOI: [10.1103/PhysRevB.80.033406](https://doi.org/10.1103/PhysRevB.80.033406). [Online]. Available: <https://link.aps.org/doi/10.1103/PhysRevB.80.033406>.
- [77] T. Feng and X. Ruan, “Quantum mechanical prediction of four-phonon scattering rates and reduced thermal conductivity of solids,” *Phys. Rev. B*, vol. 93, p. 045202, 4 Jan. 2016. DOI: [10.1103/PhysRevB.93.045202](https://doi.org/10.1103/PhysRevB.93.045202). [Online]. Available: <https://link.aps.org/doi/10.1103/PhysRevB.93.045202>.
- [78] A. Togo, L. Chaput, and I. Tanaka, “Distributions of phonon lifetimes in brillouin zones,” *Phys. Rev. B*, vol. 91, p. 094306, 9 Mar. 2015. DOI: [10.1103/PhysRevB.91.094306](https://doi.org/10.1103/PhysRevB.91.094306). [Online]. Available: <https://link.aps.org/doi/10.1103/PhysRevB.91.094306>.
- [79] A. Chernatynskiy and S. R. Phillpot, “Phonon transport simulator (phonts),” *Computer Physics Communications*, vol. 192, pp. 196–204, 2015, ISSN: 0010-4655. DOI: <https://doi.org/10.1016/j.cpc.2015.01.008>. [Online]. Available: <https://www.sciencedirect.com/science/article/pii/S001046551500017X>.
- [80] T. Tadano, Y. Gohda, and S. Tsuneyuki, “Anharmonic force constants extracted from first-principles molecular dynamics: Applications to heat transfer simulations,” *Journal of Physics: Condensed Matter*, vol. 26, p. 225402, May 2014. DOI: [10.1088/0953-8984/26/22/225402](https://doi.org/10.1088/0953-8984/26/22/225402).
- [81] R. A. Duncan, G. Romano, M. Sledzinska, *et al.*, “Thermal transport in nanoporous holey silicon membranes investigated with optically induced transient thermal gratings,” *Journal of Applied Physics*, vol. 128, no. 23, p. 235106, 2020. DOI: [10.1063/1.5141804](https://doi.org/10.1063/1.5141804). eprint: <https://doi.org/10.1063/1.5141804>. [Online]. Available: <https://doi.org/10.1063/1.5141804>.
- [82] S. Mazumder and A. Majumdar, “Monte Carlo Study of Phonon Transport in Solid Thin Films Including Dispersion and Polarization,” *Journal of Heat Transfer*, vol. 123, no. 4, pp. 749–759, Jan. 2001, ISSN: 0022-1481. DOI: [10.1115/1.1377018](https://doi.org/10.1115/1.1377018). eprint: https://asmedigitalcollection.asme.org/heattransfer/article-pdf/123/4/749/5912163/749_1.pdf. [Online]. Available: <https://doi.org/10.1115/1.1377018>.
- [83] J.-P. M. Péraud and N. G. Hadjiconstantinou, “Efficient simulation of multidimensional phonon transport using energy-based variance-reduced monte carlo formulations,” *Phys. Rev. B*, vol. 84, p. 205331, 20 Nov. 2011. DOI: [10.1103/PhysRevB.84.205331](https://doi.org/10.1103/PhysRevB.84.205331). [Online]. Available: <https://link.aps.org/doi/10.1103/PhysRevB.84.205331>.
- [84] J.-P. M. Péraud and N. G. Hadjiconstantinou, “An alternative approach to efficient simulation of micro/nanoscale phonon transport,” *Applied Physics Letters*, vol. 101, no. 15, p. 153114, 2012. DOI: [10.1063/1.4757607](https://doi.org/10.1063/1.4757607). eprint: <https://doi.org/10.1063/1.4757607>. [Online]. Available: <https://doi.org/10.1063/1.4757607>.

- [85] A. Pathak, A. Pawnday, A. P. Roy, A. J. Aref, G. F. Dargush, and D. Bansal, “McBTE: A variance-reduced monte carlo solution of the linearized boltzmann transport equation for phonons,” *Computer Physics Communications*, vol. 265, p. 108 003, 2021, ISSN: 0010-4655. DOI: <https://doi.org/10.1016/j.cpc.2021.108003>. [Online]. Available: <https://www.sciencedirect.com/science/article/pii/S0010465521001156>.
- [86] L. Yang and A. Minnich, “Thermal transport in nanocrystalline si and sige by ab initio based monte carlo simulation,” *Scientific Reports*, vol. 7, p. 44 254, Mar. 2017. DOI: [10.1038/srep44254](https://doi.org/10.1038/srep44254).
- [87] M. Mohr, J. Maultzsch, E. Dobardžić, *et al.*, “Phonon dispersion of graphite by inelastic x-ray scattering,” *Phys. Rev. B*, vol. 76, p. 035 439, 3 Jul. 2007. DOI: [10.1103/PhysRevB.76.035439](https://doi.org/10.1103/PhysRevB.76.035439). [Online]. Available: <https://link.aps.org/doi/10.1103/PhysRevB.76.035439>.
- [88] F. Memarian, A. Fereidoon, and M. Darvish Ganji, “Graphene young’s modulus: Molecular mechanics and dft treatments,” *Superlattices and Microstructures*, vol. 85, pp. 348–356, 2015, ISSN: 0749-6036. DOI: <https://doi.org/10.1016/j.spmi.2015.06.001>. [Online]. Available: <https://www.sciencedirect.com/science/article/pii/S0749603615300239>.
- [89] *Graphene – density – strength – melting point*, version 1.0. [Online]. Available: <https://material-properties.org/graphene-density-strength-melting-point/>.
- [90] A. Hemmasizadeh, M. Mahzoon, E. Hadi, and R. Khandan, “A method for developing the equivalent continuum model of a single layer graphene sheet,” *Thin Solid Films*, vol. 516, no. 21, pp. 7636–7640, 2008, ISSN: 0040-6090. DOI: <https://doi.org/10.1016/j.tsf.2008.05.040>. [Online]. Available: <https://www.sciencedirect.com/science/article/pii/S0040609008006135>.
- [91] H. Li, H. Ying, X. Chen, *et al.*, “Thermal conductivity of twisted bilayer graphene,” *Nanoscale*, vol. 6, pp. 13 402–13 408, 22 2014. DOI: [10.1039/C4NR04455J](https://doi.org/10.1039/C4NR04455J). [Online]. Available: <http://dx.doi.org/10.1039/C4NR04455J>.
- [92] M. R. B. Shahadat and A. Morshed, “A molecular dynamics study of thermal transportation of graphene sheet with various temperature,” vol. 1980, Dec. 2017. DOI: [10.1063/1.5044344](https://doi.org/10.1063/1.5044344).
- [93] X. Xu, L. Pereira, Y. Wang, *et al.*, “Length-dependent thermal conductivity in suspended single-layer graphene,” *Nature communications*, vol. 5, p. 3689, Apr. 2014. DOI: [10.1038/ncomms4689](https://doi.org/10.1038/ncomms4689).
- [94] T. Feng and X. Ruan, “Four-phonon scattering reduces intrinsic thermal conductivity of graphene and the contributions from flexural phonons,” *Physical Review B*, vol. 97, Jan. 2018. DOI: [10.1103/PhysRevB.97.045202](https://doi.org/10.1103/PhysRevB.97.045202).